Beyond Byerlee friction, weak faults and implications for slip behavior

Beyond Byerlee Friction, Weak Faults and Implications for Slip Behaviour

Collettini C.[1*], Tesei T.[2], Scuderi M.M.[1], Carpenter B.M.[3], Viti C.[4]

[1]Dipartimento di Scienze della Terra, Sapienza Università di Roma, Italy

[2]Department of Earth Sciences, Durham University, Durham, UK

[3]School of Geology and Geophysics, The University of Oklahoma

[4] Dipartimento di Scienze Fisiche, della Terra e dell'Ambiente, Università di Siena

Abstract

Some faults are considered strong because their strength is consistent with the Coulomb criterion under Byerlee's friction, $0.6 < \mu < 0.85$. In marked contrast, numerous studies have documented significant fault weakening induced by fluid-assisted reaction softening that generally takes place during the long-term evolution of the fault. Reaction softening promotes the replacement of strong minerals with phyllosilicates. Phyllosilicate development within foliated and interconnected fault networks has been documented at different crustal depths, in different tectonic regimes and from a great variety of rock types, nominating fluid-assisted reaction softening as a general weakening mechanism within the seismogenic crust. This weakening originates at the grain-scale and is transmitted to the entire fault zone via the interconnectivity of the phyllosilicate-rich zones resulting in a friction as low as $0.1 < \mu < 0.3$. Collectively, geological data and results from laboratory experiments provide strong supporting evidence for structural and frictional heterogeneities within crustal faults. In these structures, creep along weak and rate-strengthening fault patches can promote earthquake nucleation within adjacent strong and locked, rate-weakening portions. Some new frontiers on this research topic regard: 1) when and how a seismic rupture nucleating within a strong patch might propagate within a weak velocity strengthening fault portion, and 2) if creep and slow slip can be accurately detected within the earthquake preparatory phase and therefore represent a reliable earthquake precursor.

*Corresponding Author cristiano.collettini@uniroma1.it, Dipartimento di Scienze della Terra, Sapienza Università di Roma, Piazzale Aldo Moro, 5, 00185 Roma, Italy.

Keywords: fault, friction, earthquakes, rheology

Highlights

Fault friction drops from 0.6 to 0.2 when interconnected networks of phyllosilicates are present.

Fluid-assisted reaction softening is a general weakening mechanism within the seismogenic crust.

The integration of geological data and results from laboratory experiments depicts structural and frictional heterogeneities within crustal faults.

Beyond Byerlee friction, weak faults and implications for slip behaviour

1. Introduction 3

2. Anderson-Byerlee frictional fault mechanics and strong faults 3

2.1 Anderson-Byerlee frictional fault mechanics *3*

2.2 Supporting evidence for Byerlee friction *5*

2.3 Structural and mechanical characteristics of strong faults *7*

3. From strong to weak faults

3.1 Weak-fault structure *10*

3.2 Reaction softening *13*

3.3 Frictional properties of phyllosilicate-rich faults *19*

4. Discussion 23

4.1 Structural and frictional heterogeneous crustal faults *23*

4.2 Fault patches interaction during tectonic loading *27*

4.3 Some challenging topics *28*

Acknowledgements 31

References 32

Table 1 46

Table 2 48

1. Introduction

For years, there have been lines of evidence that inform the weak vs. strong fault debate. Robust evidence exists that indicates that some crustal faults are strong whereas others are weak. However in the last ten years, the classification of faults as strong or weak seems to have been replaced by the idea that faults are structurally and frictionally heterogeneous. Fault heterogeneities have been mainly proposed on the grounds of field geology, frictional measurements of different natural fault rocks, seismicity distribution, frequency content of seismic waveforms and geodetic imaging of active faults. In this review we begin by presenting supporting evidence for strong faults and their associated internal structure. Then we will show examples of weak faults together with the physico-chemical processes at the origin of fault zone weakness, and report on the frictional properties as measured in the laboratory. In the discussion we merge observations from the internal structure of strong and weak faults with their frictional properties to: a) derive an integrated view of a structural and frictional heterogeneous crustal scale fault; and b) discuss how heterogeneous fault patches might interact during tectonic loading.

An important point worth mentioning in the introduction is that by fault zone weakening processes we mean processes occurring mainly during the entire fault history (hundreds to millions of years), and for fault weakness we refer to a very low steady-state fault frictional strength. This low frictional strength is generally measured in laboratory experiments at low sliding velocities, i.e. 0.01 μm/s < v < 100 μm/s, and can be used as a proxy to evaluate the fault strength during the interseismic or pre-seismic phases of the seismic cycle. Therefore, the important dynamic weakening mechanisms that occur during the earthquake slip and induced by temperature rise at high slip velocities are not considered in our analysis.

2. Anderson-Byerlee frictional fault mechanics and strong faults

2.1 Anderson-Byerlee frictional fault mechanics

The strength evaluation of faults contained within the crust requires both a measure of the resolved stress on the fault plane and a quantifiable model for the failure threshold. E. M. Anderson in his seminal paper of 1905 and in his memoirs of 1951 developed groundbreaking research on this topic. He identified three tectonic regimes together with the orientation of the faults within these regimes, laying the foundations for fault strength evaluation. The Andersonian theory of faulting is based on three main assumption: a) the crust is

102 homogeneous and isotropic; b) one principal stress is vertical since the Earth's surface is a
103 free surface; and c) brittle faults form in accordance with the Coulomb criterion for shear
104 failure:
105
106 $\tau = C + \mu_i \sigma'_n = C + \mu_i (\sigma_n - P_f)$ (1)
107
108 where τ and σ_n are, respectively, resolved shear and normal stresses on the failure plane, C is
109 the cohesive strength, μ_i is the coefficient of internal friction, (C and μ_i are rock material
110 properties) and Pf is the pore fluid pressure. However with increasing displacement the
111 cohesive strength of a fault is very small compared to the shear and normal stresses to be
112 neglected and the internal friction coefficient is replaced by a sliding friction coefficient, μ_s,
113 resulting in the Amontons' law:
114
115 $\tau = \mu_s (\sigma_n - P_f)$ (2)
116
117 At this point, assuming hydrostatic fluid pressure, a characterization of the sliding friction
118 coefficient is required for fault strength evaluation. In 1978 J. Byerlee published an extensive
119 dataset of laboratory friction measurements showing that friction is nearly independent of
120 the rock type and is in the range $0.6 < \mu_s < 0.85$. This experimental friction range is commonly
121 known as the Byerlee's rule of friction and the near 4000 citations in Google Scholar received
122 so far by the 1978 paper testifie to the great impact and widespread use of the Byerlee's rule.
123
124 *2.2 Supporting evidence for Byerlee friction*
125 Once provided experimental support for μ_s another important question is whether such
126 friction coefficients, $0.6 < \mu_s < 0.85$, obtained from laboratory experiments using centimetric
127 or millimetric samples, also hold for large-displacement faults in the crust with dimensions of
128 several kilometres or larger. Two lines of evidence support the applicability of Byerlee friction
129 to crustal faults.
130 The first evidence is produced by the dip distribution of moderate-to-large ruptures in
131 extensional and compressional environments that seem to be controlled by frictional fault
132 reactivation theory under Byerlee friction (Sibson, 1985; Collettini and Sibson, 2001). For the
133 two-dimensional case in which an existing fault containing the σ_2 axis lies at a reactivation
134 angle, θ_r, to σ_1, equation 2 may be written in term of principal stresses as:

$$R = \frac{(\sigma_1 - P_f)}{(\sigma_3 - P_f)} = \frac{(1+\mu_s \cot\theta_r)}{(1-\mu_s \tan\theta_r)} \quad (3)$$

defining the relative ease of reactivation for faults at varying angles to σ_1 (Sibson, 1985), where σ_1, σ_2 and σ_3 are the maximum, intermediate and minimum principal stresses respectively. The optimal orientation for frictional reactivation is given by $\theta^*_r = 0.5\tan^{-1}(1/\mu_s)$. As θ_r increases or decreases away from this optimal position, the stress ratio required for reactivation increases. Frictional lock-up ($R \rightarrow \infty$) occurs when $\theta^*_r = 2\,\theta^*_r \tan^{-1}(1/\mu_s)$. For Byerlee's friction range, optimal reactivation occurs when $\theta_r = 25°–30°$ and frictional lockup is expected at $\theta_r = 50°–59°$.

Figure 1 shows the dip distribution of reverse and normal fault ruptures obtained from focal mechanisms of shallow, intracontinental earthquakes (M > 5.5; slip vector raking 90° ± 30° in the fault plane) where the rupture plane is unambiguously discriminated. On the same figure, under the assumption of vertical and horizontal σ_1 trajectories for extensional and compressional regimes, respectively, the dip distributions, δ, of ruptures are plotted also as functions of the reactivation angle, θ_r. The cut-off at $\theta_r \approx 60°$ for both varieties of dip-slip faults is consistent with frictional lockup for $\mu_s = 0.6$, at the bottom of the Byerlee range. Lower coefficients are possible, but $\mu_s = 0.6$ is also consistent with the dominant peak at $\theta_r \approx 30°$ in the reverse-slip distribution representing the optimal orientation for reactivation. The absence of this peak for normal faults is explicable by: a) the different reactivation curves for the two faulting modes with a more acutely defined minimum at optimal orientation for reverse faults than for normal faults (Collettini and Sibson, 2001); and b) the significant number of normal faults ruptures obtained from earthquakes occurring in central Italy and nucleating on faults forming with dip angles of 45° as ductile shear zones following planes of maximum shear stress (Collettini et al., 2009a). The dataset and frictional analysis presented in figure 1 provide strong evidence for seismogenic faults possessing sliding friction coefficient similar to those measured in the laboratory by Byerlee, but see also contradictory observations for earthquakes occurring in the oceanic lithosphere (Craig et al., 2014; Tesei et al., 2018) or microseismicity along low-angle normal faults (Collettini, 2011). The fact that some faults are reactivated close to frictional lock-up also implies that localized fluid overpressure may be needed for reactivation.

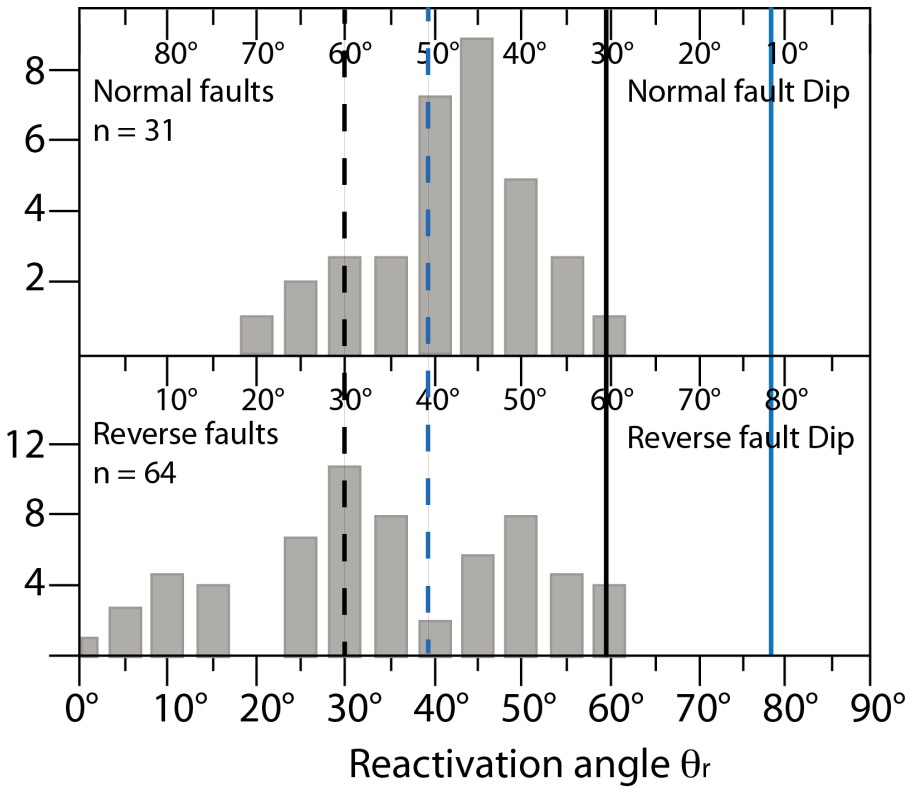

Figure 1. A constraint on Byerlee friction from the dip of the earthquake ruptures. Dip distribution of normal and reverse fault ruptures obtained from focal mechanisms of shallow, intracontinental earthquakes where the rupture plane is unambiguously discriminated (from compilations of Jackson and White 1989; Sibson and Xie, 1998; Collettini and Sibson 2001; Sibson 2009), with the addition of 6 extensional earthquakes from Italy occurring during the L'Aquila 2009 and central Italy 2016-2017 seismic sequences (details in Chiaraluce, 2012; Chiaraluce et al., 2017; cnt.rm.ingv.it). Within an Andersonian stress field, for normal faults, θ_r = 90°- δ, and for reverse faults, θ_r = δ, where δ is the fault dip angle. The vertical lines mark optimal orientation (dashed line) and frictional lock-up (solid line) for a friction coefficient of μ_s = 0.6 (black lines) and μ_s = 0.2 (blue lines).

The second evidence for the applicability of Byerlee friction to crustal faults derives from in-situ measurements of the state of stress in the crust. One of the first places where frictional faulting was demonstrated to be clearly applicable to faulted crust was the Yucca Mountain area in Nevada. Here the magnitudes of the least principal stress, measured at different depths, are consistent with frictional fault reactivation, summarized in equation 2, for a friction coefficient of $\mu_s \approx 0.6$ (Zoback and Healy, 1984). On the same line of evidence, a comprehensive compilation of stress measurements, in relatively deep boreholes from different tectonic environments and through different rock types, shows that the measured stress magnitudes are consistent with the values predicted by the Coulomb criterion for hydrostatic fluid pressure and for friction coefficients within the Byerlee's experimental range (Townend and Zoback, 2000). In normal faulting stress fields, borehole stress measurements in sedimentary basins are consistent with the Coulomb criterion for a friction of $\mu_s \approx 0.6$

(Zoback, 2010). Examples are documented in Texas within different rock types like sandstone, siltstone, shale and limestones, in the North Sea within chalk and in the Gulf of Mexico within sand reservoir. More recently the induced seismicity crisis in Oklahoma and southern Kansas have provided a unique opportunity to better characterize the reactivation of dormant faults under anthropogenic forcing. The widespread occurrence of seismicity despite very modest pressure changes in the basement and the observation that the activated faults are well oriented within the contemporary stress field (Walsh and Zoback, 2016; Schoenball and Ellsworth, 2017) provide strong support for the hypothesis of a critically stressed strong crust with hydrostatic fluid pressure and Byerlee friction (e.g. Townend & Zoback, 2000).

2.3 Structural and mechanical characteristics of strong faults

The localization of strain along crustal faults produces a fault structure that generally consists of a fault core, where most of the deformation is localized, surrounded by a damage zone formed by distributed fractures and subsidiary, small displacement faults (e.g. Chester et al., 1993). Cataclastic deformation (brittle fragmentation by macroscopic fracturing and grain comminution) intensifies toward the fault core that consists of one or more tabular zones of ultracataclasite, within which bands of intense grain-size reduction define principal slip zones (e.g. Sibson, 1977; Chester and Chester, 1998). A comprehensive characterization of fault zone structure is beyond the scope of the present manuscript and it is well described in several excellent review papers such as Caine et al., (1996), Ben-Zion and Sammis, (2003), Sibson (2003), Wibberley et al., (2008) and Faulkner et al., (2010). Here we try to link structural and mechanical data in order to summarize the main mechanical characteristics of strong faults.

Several faults hosted within crystalline rocks show cataclastic deformation with grain size reduction and localization along discrete slipping surfaces (e.g. Fig. 2a and Smith et al., 2013). The preservation of pseudotachylites within some of these shear zones (Sibson 1977; Swanson 2006; Di Toro and Pennacchioni 2005; Spray, 2010) testifies to earthquake occurrence along these structures. The San Gabriel fault, within the San Andreas fault system, has an heterogeneous fault structure that in some localities is constituted by a fault core with significant slip localization along ultracataclasite layers made of quartz and feldspars (Evans and Chester, 1995). A classical example of extreme localization has been documented for the Punchbowl fault (Chester and Chester, 1998), with a 1 mm thick principal slip zone consisting of < 100 nm particles (Chester et al., 2005). Dynamic weakening mechanisms (e.g. Rice, 2006; Di Toro et al., 2011) favoured by extreme localization have been invoked (Chester and

224 Chester, 1998) to explain the weakness of the San Andreas: in this view the fault would be
225 statically strong yet dynamically weak (Rice et al., 2009). Some faults that cross-cut silica-rich
226 sediments, like the Corona Heights fault, in San Francisco, show a mirror-like finish due to the
227 presence of 1-3 mm thick zone of vitreous silica formed during earthquake slip (Kirkpatrick et
228 al., 2013). Faulting within sandstones results in one or more through-going slip surfaces
229 where the great part of the displacement is accommodated by quartz grain-size reduction and
230 localization along principal slip surfaces (Shipton and Cowie, 2001). The Pretorius fault in Tau
231 Tona mine, South Africa, during its Archaean activity, experienced multiple slip events along a
232 quartz-rich principal slip surface and in 2004 it was reactivated by a M = 2.2 earthquake. The
233 mapped earthquake rupture at 3.6 km of depth reveals that the seismic slip produced 1-5 mm
234 thick fault gouge along four quasi-planar segments of the ancient fault-zone (Heesakkers et al.,
235 2011). Faulting within massive carbonates (Fig. 2b) is characterized by localization along sub-
236 parallel slipping zones where the deformation is localized along very thin (< 500 μm) zones
237 bounded by mirror-like slipping surfaces (De Paola et al., 2008; Fondriest et al., 2013; Siman-
238 Tov et al., 2013; Collettini et al., 2014). In some of these carbonate-bearing faults, calcite
239 crystals exhibiting localized disaggregation together with a high concentration of vesicles
240 indicate thermal decomposition during past earthquakes (e.g. Rowe et al., 2012; Collettini et
241 al., 2013). In other structures nanograins texture with polygonal grain boundaries suggest
242 superplastic deformation of carbonates during earthquake-slip (De Paola et al., 2015).
243

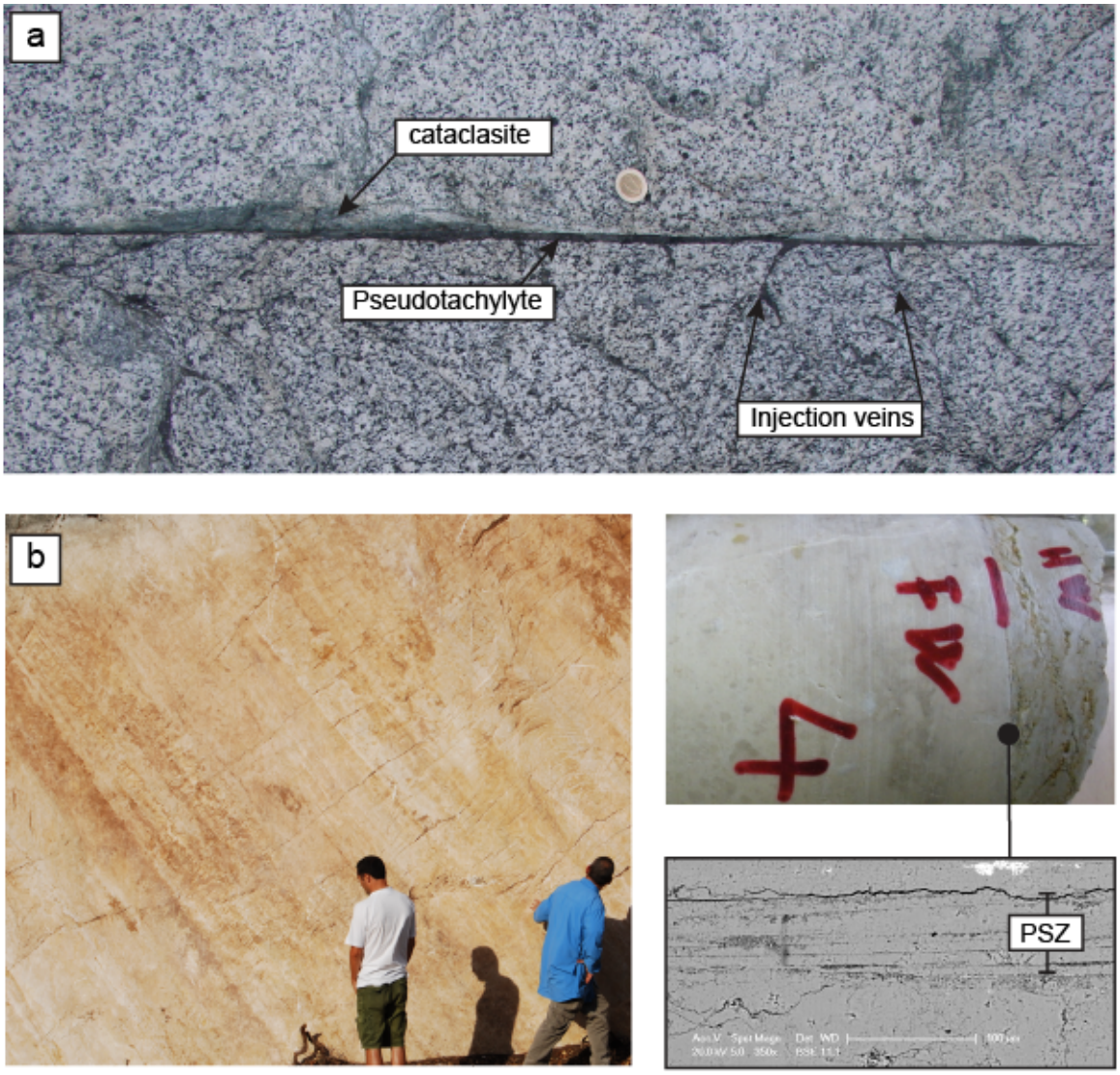

Figure 2. Strong faults. a) Pseudotachylyte-bearing fault from the Gole Larghe outcrop in the Italian Alps (Di Toro and Pennacchioni, 2005; Smith et al., 2013). Cataclasite- and pseudotachylyte-bearing faults surround relatively intact blocks of tonalite, and pseudotachylyte overprints cataclasites. b) Mirror-like slip surface from the Monte Maggio fault in the Apennines of Italy (Collettini et al., 2014). The panels on the right show localized deformation along a sharp slipping zone, affected by grain-size reduction and thermal decomposition processes (localized disaggregation with a high concentration of holes) along the Principal Slipping Zone, PSZ; Scanning Electron Microscope, SEM, image.

3. From strong to weak faults

The datasets presented above support the interpretation that crustal faults in general fail according to equation (2) with μ_s = 0.6 – 0.85 and hydrostatic fluid pressure. These structures represent strong faults since the differential stress, (σ_1 - σ_3), or the shear stress required for their reactivation is quite high. At 10 km of depth (σ_1 - σ_3) > 100 MPa and it increases significantly from extensional to compressional environments (Sibson, 1974); for example in

the KTB borehole the differential stress at 9 km of depth is about 170 MPa (Townend and Zoback, 2000).

However, several observations cast doubt on the fact that deformation within the crust is exclusively controlled by strong faults and amongst these, we report the two that we consider the most relevant. First, there is an important number of faults that experience reactivation although they are severely misoriented within the regional stress field. Examples of these structures are given by the San Andreas fault in a strike slip regime (Zoback et al., 1987; Carpenter et al., 2011; Lockner et al., 2011), low-angle normal faults in extensional environments (Wernicke, 1981; Collettini 2011) and sub-horizontal thrusts in compressional regimes (Price, 1988; Davis et al., 1983; Suppe 2007; Tesei et al., 2015). Reactivation along these structures is possible only following significant fault weakening that can be achieved by either an increase in fluid pressure, or a reduction in friction coefficient or a combined effect (e.g. Hubbert and Rubey, 1959; Rice, 1992; Faulkner et al., 2006; Suppe 2007; Tesei et al., 2015). Second, in the last 15 years, geophysical observations combined with numerical models have shown that aseismic creep is common and sometimes prevalent within the seismogenic layer (e.g. Avouac, 2015), and a continuum spectrum of fault slip behaviour, including slow slip phenomena, can be present at all depths of crustal faults (e.g. Bürgmann, 2018). This richness in fault slip behaviour for crustal faults is difficult to be captured only by strong faults with Byerlee friction.

3.1 Weak-fault structure

In marked contrast to strong faults, there is a significant number of crustal structures showing distributed deformation along interconnected, anastomosing shear zones rich in phyllosilicates. The geometry and internal fabric of these shear zones strongly resembles, and is sometimes derived from, ductile shear zones of high metamorphic grade (e.g. Berthé et al., 1979; Platt and Vissers, 1980). In this paragraph we will present some well-documented field examples of phyllosilicate-rich crustal faults (Fig. 3 and Table 1).

For strike-slip faulting, the Carboneras fault in Spain (Fig. 3a) is characterized by 1 km thick fault core consisting of foliated and interconnected networks of phyllosilicate-rich zones (Faulkner et al., 2003; Rutter et al., 2012). These anastomosing networks are up to 50 m thick and are rich in chlorite and illite derived from a mica schist protolith (Solum and van der Pluijm, 2009). The creeping section of the San Andreas fault at SAFOD consists of multiple fault strands, made of foliated serpentinite and smectite clays (Holdsworth et al., 2011), that

294 are several meters wide and creep simultaneously (Zoback et al., 2010). Some segments of the
295 Median Tectonic Line in Japan consist of several meters thick, foliated fault rocks rich in
296 chlorite (Wibberley and Shimamoto, 2003; Jeffereis et al., 2006). During the final activity of
297 the fault at shallow crustal levels the deformation is concentrated along clay rich shear zones
298 (Wibberley and Shimamoto, 2003). Exhumed shallow portions of the North Anatolian fault
299 are characterized by hundreds of meter thick faults where the deformation is mainly
300 accommodated within sub-parallel shear-zones rich in talc, kaolinite and chlorite (Kaduri et
301 al., 2017). The Livingstone fault zone in New Zealand (Tarling et al., 2018) is dominated by a
302 serpentinite mélange tens to several hundreds of metres wide, in which a pervasive
303 anastomosing fabric surrounds pods of more competent material (e.g., metasediments,
304 rodingite, massive serpentinite) ranging from tens to hundreds of metres in size. The foliated
305 serpentinite shear zone is mostly made of fibrous serpentine and lizardite, consistent with the
306 estimated ambient temperature during shearing of 300–350 °C.
307
308 For thrusts faults there are plenty of examples of foliated phyllosilicate-rich shear zones.
309 Notable examples may include the classic phyllonites associated to the Moine thrust zone,
310 possibly formed by retrogression and shearing of mylonitic gneissose protoliths under lower
311 greenschist facies conditions (McClay and Coward, 1981, Wibberley, 2005). Other examples of
312 phyllonitic fault rocks have been documented in the Karakoram fault zone in the Himalayas
313 (Wallis et al., 2015) or along the Red River shear zone in the Yunnan Province in China (e.g.
314 Wintsch and Yeh, 2013). The Perdido thrust in the Pyrenees consists of a several meters thick
315 and foliated shear zone, rich in illite and chlorite (Lacroix et al., 2011), separating more
316 competent lithologies in the hanging-wall (limestones) and footwall (turbidites sandstone).
317 The Monte Fico thrust in the Elba Island in Italy (Fig. 3b) is a c. 200 m thick shear zone formed
318 by competent lenses of retrograde pseudomorphic serpentinite surrounded by an
319 anastomosing network of foliated serpentinites (Viti et al., 2018). Several tectonic mélanges
320 around the world, thought to constitute exhumed analogues of subduction channels, are
321 constituted by anastomosing shear zones enriched in phyllosilicates enveloping lenses of
322 more competent lithologies (e.g. Cowan, 1974; Byrne et al., 1988; Cloos and Shreve, 1988,
323 Kimura et al., 2012; Morley et al., 2017; Rowe et al., 2013). For instance, the Rodeo Cove
324 thrust, near San Francisco, consists of a 200 m thick shear zone with a foliated fabric rich in
325 chlorite that formed at about 8-10 km of depth (Meneghini and Moore, 2008). The Chrystalls
326 Beach Complex accretionary mélange of New Zealand (Fagereng and Sibson, 2010) consists of
327 competent lenses of chert, sandstone and metabasalts surrounded by an interconnected

network of phyllosilicates, i.e. illite-muscovite, developed at depth < 300°T (Fagereng and Cooper, 2010). At shallower crustal levels other examples of tectonic mélange are reported in Vannucchi et al., (2012 and references therein). In the Apennines of Italy, in marly limestones, shear zones formed at crustal depths < 4 km show a thickness ranging from several to hundreds of meters with concentration of illite and smectite within the interconnected and foliated network of the fault core (e.g. Koopman, 1983; Tesei et al., 2013).

Some large displacement extensional faults formed in the US within quartz-feldspatic rocks reveal a heterogeneous structural zonation with fault zone thickness ranging from < 10 m for the Mineral Mountains fault to locally about 20 m for segments of the Wasatch and Dixie Valley faults (Bruhn et al., 1994). The fault zone is made of fault breccia, fine-grained cataclasites and foliated zones rich in muscovite, biotite, chlorite and clays. Some portions of the Zuccale low-angle normal fault in Italy, consist of an up to 8 m thick fault core rich in talc and smectite (Collettini et al., 2011). The Black Mountains detachment in California shows deformation that is asymmetrically distributed, increasing upward from the footwall (Cowan et al., 2003). A well-defined slip zone separates hangingwall Quaternary fanglomerates from fault rocks consisting of foliated fault breccia and fault gouge where weak mineral phases (illite, chlorite, smectite and saponite) are concentrated (Hayman, 2006). The Gubbio normal fault in the Apennines of Italy shows some segments characterized by foliated SC fabric from the metric (Fig. 3c) to the microscale. These segments form predominantly within marly carbonates and show the concentration of clays within the shear zone (Bullock et al., 2014). The Err Nappe detachment in Switzerland shows a fault core made of a continuous layer of black gouge, with thickness ranging from a few centimetres to some metres (Manatschal, 1999). In the footwall the granitic host rock is affected by brittle fracturing associated with a complex vein system and towards the fault core fluid-assisted diffusion mass transfer processes occurring under lowermost greenschist facies conditions promoted the development of an SC fabric rich in chlorite and illite (Manatschal, 1999).

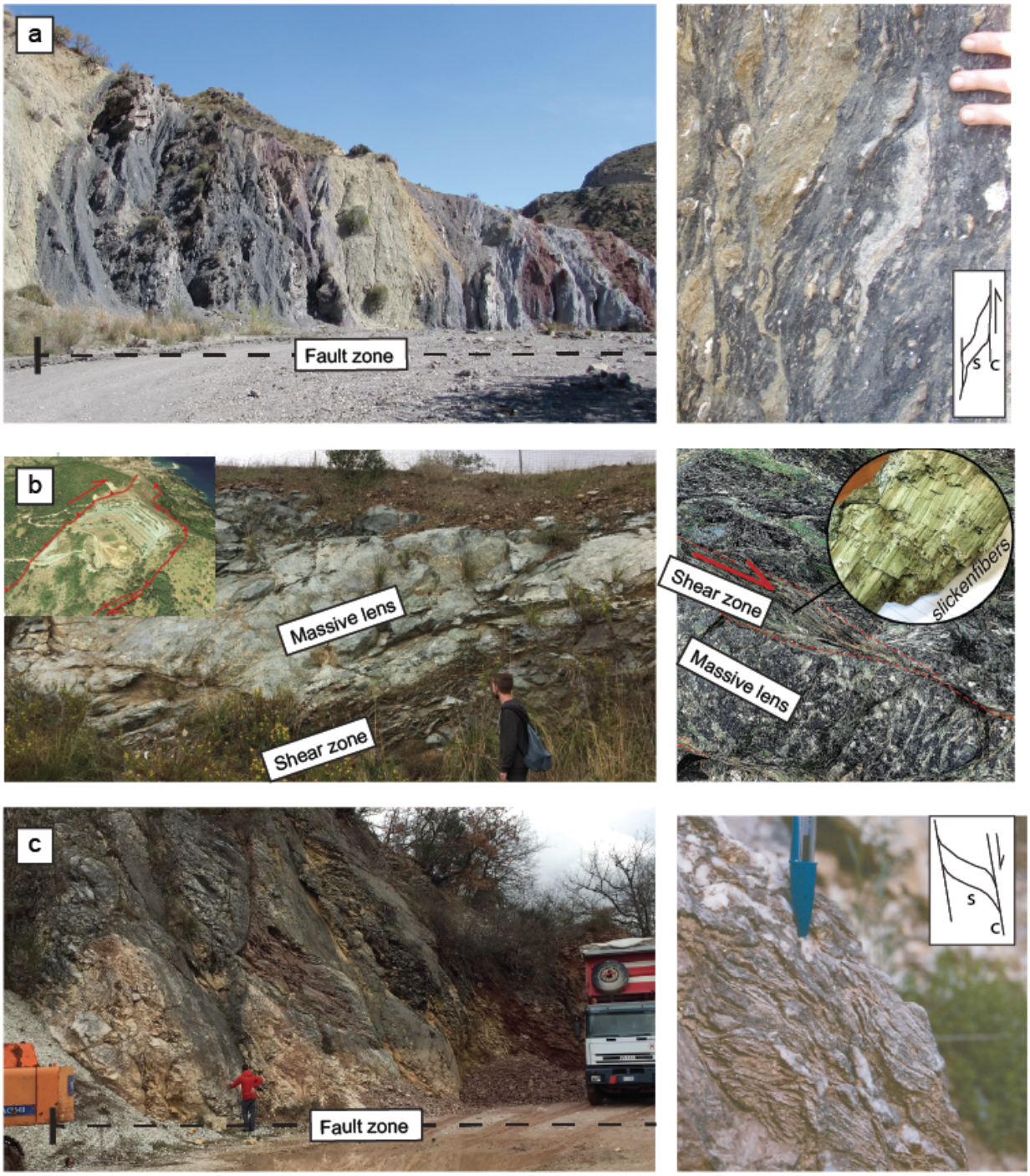

Figure 3. Weak faults. a) Outcrop view of the Carboneras fault SE Spain (Faulkner et al., 2003; Rutter et al., 2012). Each of the coloured bands represents different types of fault gouge that have been juxtaposed due to movements on the fault. The image on the right shows details, in map-view, of the SC fabric with left-lateral kinematics. The fault rock consists of a clay-bearing gouge derived from graphitic mica schist (Rutter et al., 2012). b) The Monte Fico thrust (Elba Island, Italy) is a 200m thick structure (panoramic view in the inset) characterized by SCC' fabric. Sigmoidal competent lenses of serpentinites are surrounded by shear-zones coated with fibrous serpentine and lizardite (Tesei et al., 2018; Viti et al., 2018). c) Gubbio normal fault in the Apennines of Italy. In this outcrop the fault is up-to 30 m wide and is characterized by an SCC' fabric at the metric and centimetric scale (details in Bullock et al., 2014).

3.2 Reaction softening

Fault zone architecture exerts a primary control on fluid flow in crustal shear zones (Sibson, 1992; Caine et al., 1996; Wibberley et al., 2008; Faulkner et al., 2010). The influx of fluids into fault zones can trigger two main types of weakening process that operate over different timescales. In the short term of the seismic cycle, crustal fluids can be trapped within low-permeability fault zones promoting the development of fluid overpressure, e.g. the mechanical weakening that reduces the effective normal stress (equation 2 and Hubbert and Rubey, 1959). During the entire fault history fluid circulation within shear zones might exert a chemical role facilitating the replacement of strong mineral phases with weak mineral phases, hence promoting reaction softening (e.g. Janecke and Evans, 1988; Bruhn et al., 1994; Evans and Chester, 1995; Wintsch et al., 1995; Manatschal, 1999; Imber et al., 1997; Wibberley, 1999; Collettini and Holdsworth 2004; Schleicher et al., 2010; Warr et al., 2014). In the following we will review some examples of fluid assisted reaction softening generated in different protoliths and occurred at different crustal levels. Then we will integrate these observations in a general mechanism for fluid assisted fault weakening.

In the thrusts of the Apennines, when shear zones develop within marly limestones, faults with kilometric displacement show distributed deformation along thick (up to 200 m) shear zones (Fig. 4a and Tesei et al., 2013) characterized by SCC' fabric (e.g. Ramsay and Graham, 1970; Berthé et al., 1979; Bos and Spiers, 2001 and Fig. 4b). The evolution of the fault zone structure, inferred from the analysis and comparison of small, intermediate and kilometric displacement faults, indicates that during the early stages of deformation dissolution of the carbonates favours the concentration of insoluble clay minerals within stylolitic surfaces (Fig. 4c, Tesei et al., 2013; Gratier et al., 2013; Lacroix et al., 2015). With increasing deformation the stylolites evolve into an interconnected foliation (Fig. 4d, see also Gratier and Gamond, 1990), formed by smectitic clays in nanosized (001) lamellae (Fig. 4e) with preferred orientation parallel to the local slipping surface (Viti et al., 2014). Foliation parallel veins (Fig. 4c) with crack-and-seal texture, suggest that the low permeability and the anisotropy of clay fabric favoured cyclic fluid overpressure development during the fault activity.

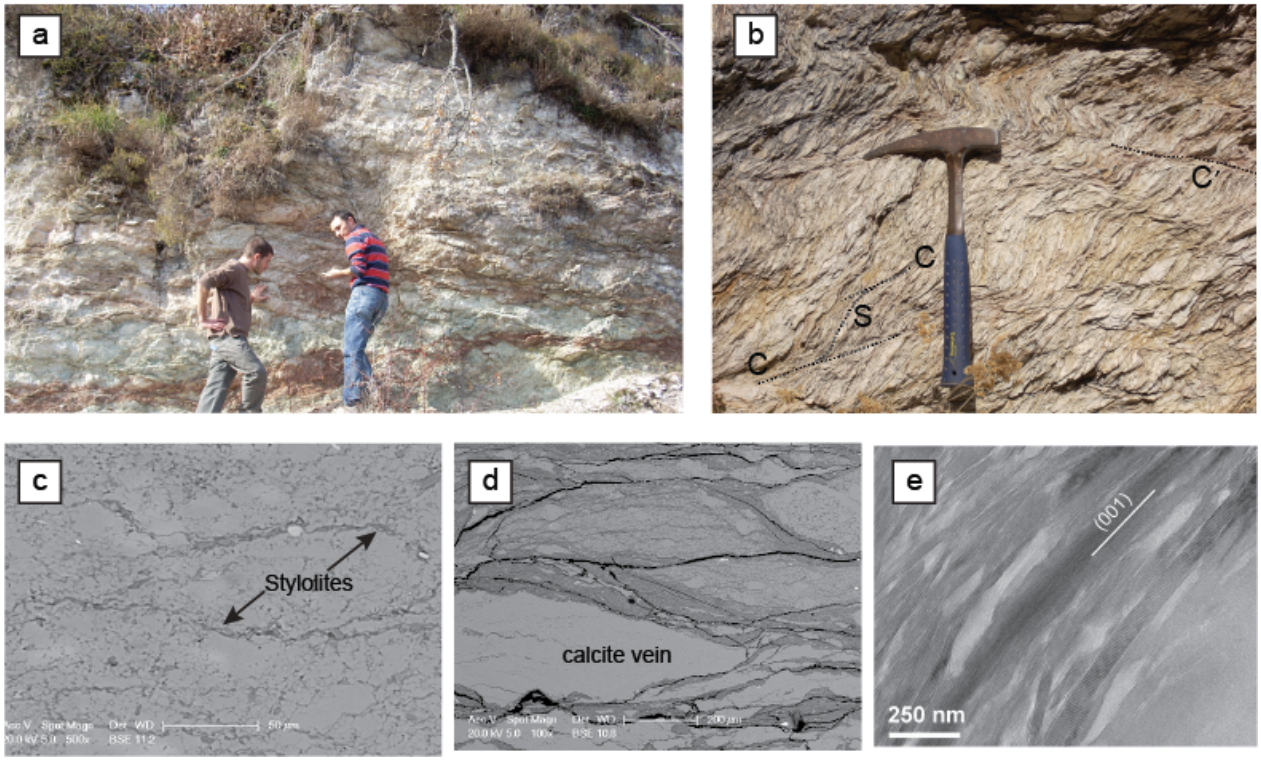

Figure 4. Fault weakening in marly limestones. a) and b) In the exposed outcrop, the Coscerno thrust (Northern Apennines of Italy) is ≈20 m thick and is characterized by a fault rock showing a pervasive SCC' fabric (e.g. Tesei et al., 2013). c) From a marly protolith, characterized by calcite (light grey) with a small amount of clay (heavy grey), dissolution of calcite favours the concentration of insoluble clays initially along stylolites. d) In mature fault rocks the clay minerals form interconnected networks, with calcite veins parallel to the foliation. In some cases these veins a re-worked by dissolution processes. e) Within the interconnected clay-rich networks, the deformation is accommodated by frictional sliding along smectite lamellae nearly parallel to the sense of shear. c) and d) are Scanning Electron Microscope, SEM, images and e) is a Transmission Electron Microscope, TEM, image.

Along the Zuccale low-angle normal fault (Elba island, Italy) during the initial phase of deformation, fracturing of a dolomitic protolith favoured the influx of silica-rich fluids into the fault zone. In the low-strain domains fluids interacted with the fine-grained cataclasite promoting dissolution of the dolomite and precipitation of talc (Collettini, et al., 2009c). In the high-strain domains the mature fault zone structure consists of an interconnected foliated network (Fig. 5a-c) that deforms by frictional sliding along 50–200 nm-thick talc and smectite lamellae (Fig. 5d and Viti and Collettini, 2009). Here again foliation-parallel veins (Fig. 5b) indicate fluid involvement and fluid overpressure development during the fault activity.

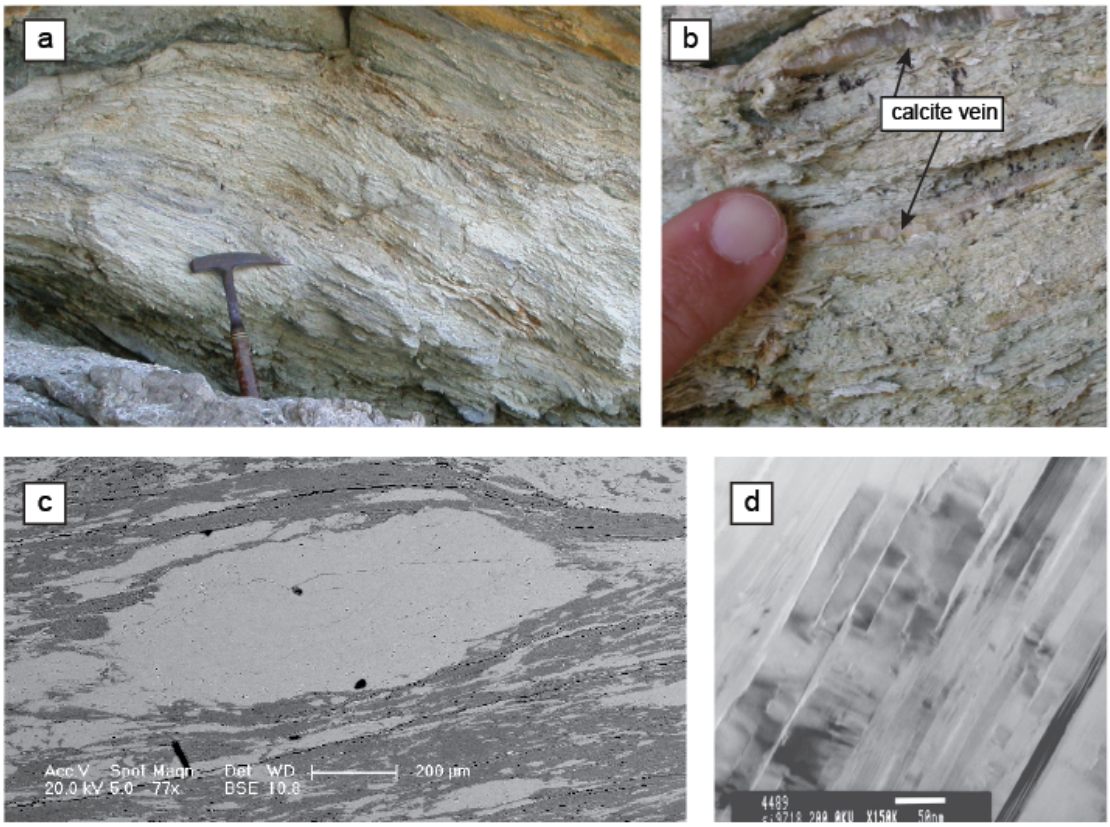

Figure 5. Fault weakening in dolostones. a) Talc-rich foliated structure of the Zuccale low-angle normal fault in the Elba Island, Italy (Collettini et al., 2009c). b) Detail of the foliated fault rock with foliation parallel calcite veins. c) SEM image showing sigmoids of calcite, light grey, within interconnected talc-rich foliated microstructure, heavy grey. d) TEM image showing interlayer delamination and frictional sliding along talc (001) lamellae (Viti and Collettini, 2009).

The Moonlight Fault in southern New Zealand consists of a 20 m thick shear zone formed within grey and green schists. Microstructural studies suggest that in the early stages of the fault activity brecciation promoted grain-scale dilatancy favouring the influx of hydrous fluids into the fault zone (Fig. 6 and Alder et al., 2016). Seams of fine-grained insoluble phyllosilicates that anastomose clasts of quartz and albite, and overgrowth of chlorite indicate that the shear zone deformed by dissolution - precipitation mechanisms that accompanied frictional sliding along the phyllosilicate foliae. In the high strain domains of the shear zone it is evident a high concentration of chlorite and muscovite derived from the hangingwall green-schists and footwall grey-schists respectively (Fig. 6 and Alder et al., 2016). Similar weakening processes in quartz-feldspatic rocks have been extensively documented in other fault zones worldwide in Janecke and Evans, (1988), Bruhn et al., (1994), Evans and Chester, (1995), Wintsch et al., (1995), Wibberley, (1999), Imber et al., (1997), Wintsch and Yeh, 2013 and Wallis et al., 2015.

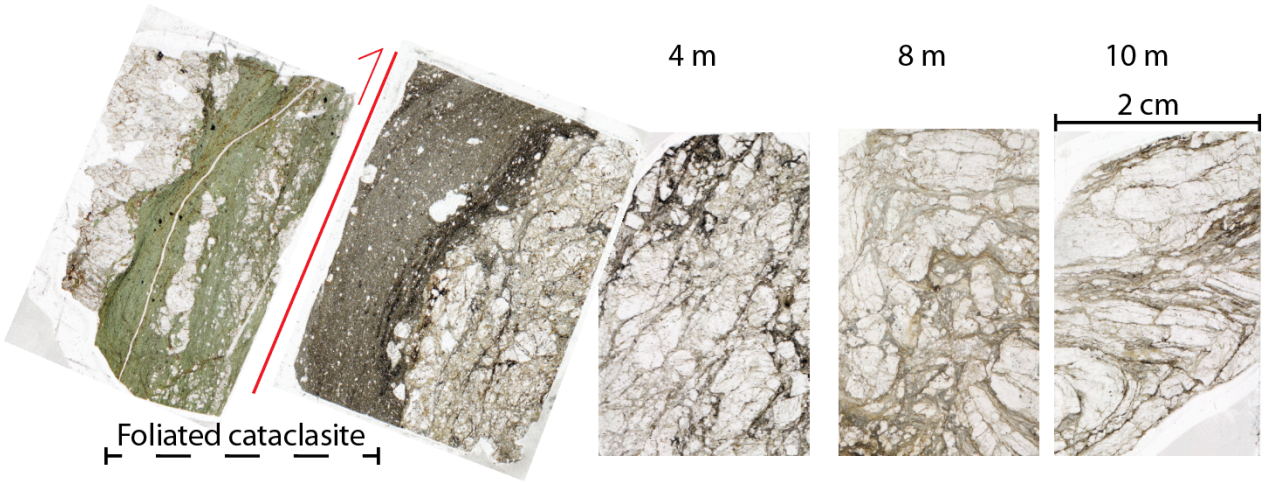

Figure 6. Fault weakening in quartz-feldspatic schists. The Moonlight fault in New Zealand shows a fault core containing an up to 20 m thick sequence of breccias, cataclasites and foliated cataclasites. Series of scanned thin sections from samples collected at distances of <10 m from the shear zone illustrating the progression of deformation towards the fault core via a: 1) decrease in grain-size/increase in matrix proportion; 2) modal increase in abundance of phyllosilicates; 3) increasing alignment of phyllosilicate lamellae, chlorite in green and muscovite in black. Modified from Alder et al., 2016.

In ultramafic rocks different stages of weakening have been documented. Brittle fracturing and grain-size reduction is a fundamental process in the early stages of peridotite serpentinisation, because it promotes the formation of fluid pathways and allows for efficient interface hydration reactions of primary peridotitic minerals (Plumper et al., 2012). Serpentinisation results in pseudomorphic textures (mesh cores/rims and bastites, from olivine and pyroxene, respectively), consisting of a mixture of lizardite, chrysotile and polygonal serpentine (e.g. Escartin et al., 2001). In retrograde serpentinites, during shear deformation, two main processes favour further progressive weakening (Fig. 7 and Viti et al., 2018): 1) preferential dissolution of mesh cores favours the development of an interconnected network of sub-parallel lizardite lamellae with (001) planes parallel to the shear direction; and 2) subsequent precipitation promotes the development along shear zones of fibrous serpentines (chrysotile and polygonal serpentine) with the fibre axis oriented parallel to the shear direction (Fig. 7 c). Frictional sliding along (001) lizardite lamellae or along fiber axis of fibrous serpentinites results in a friction of $0.15 < \mu_s < 0.19$ (Tesei et al., 2018).

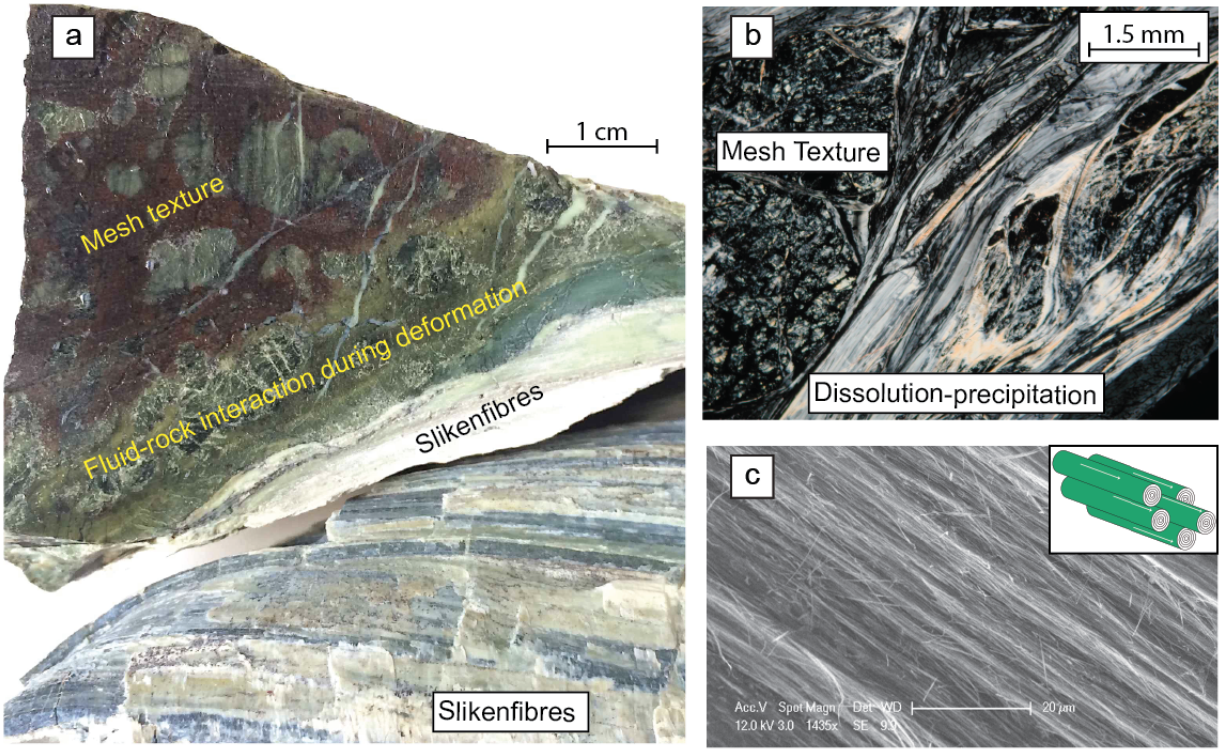

Figure 7. Monte Fico fault in Elba island, Italy: fault weakening in ultramafic rocks. a) Hand sample showing the transition from the mesh texture to the slikenfibers coating the shear zones. b) Mesh texture and slikenfibers at the optical microscope. c) Parallel fiber axis of fibrous serpentines, SEM image (details in Tesei et al., 2018; Viti et al., 2018).

Collectively the examples of fault evolution reported above indicate that in the early stages of deformation, brittle fracturing favours the increase of fault zone permeability promoting the influx of fluids into the fault zone (Fig. 8a). Fluids interact with the fine-grained portions of the cataclasites (Fig. 8b) and promote dissolution and precipitation processes that favour the replacement of strong mineral phases (quartz, feldspar, olivine, pyroxene, calcite, dolomite) with weak mineral phases (clays, talc, chlorite, muscovite, lizardite, fibrous serpentine). With increasing deformation, this fluid assisted reaction softening, allows the development of an interconnected and phyllosilicate-rich microstructure where a significant amount of slip is accommodated by frictional sliding along the phyllosilicate foliae (Fig. 8c). The development of foliated networks rich in platy minerals makes the fault a low permeability barrier that can trap crustal fluids and generate fluid overpressures as suggested by the numerous veins documented parallel to the foliated networks (e.g. Fig. 4d, 5b, 7b).

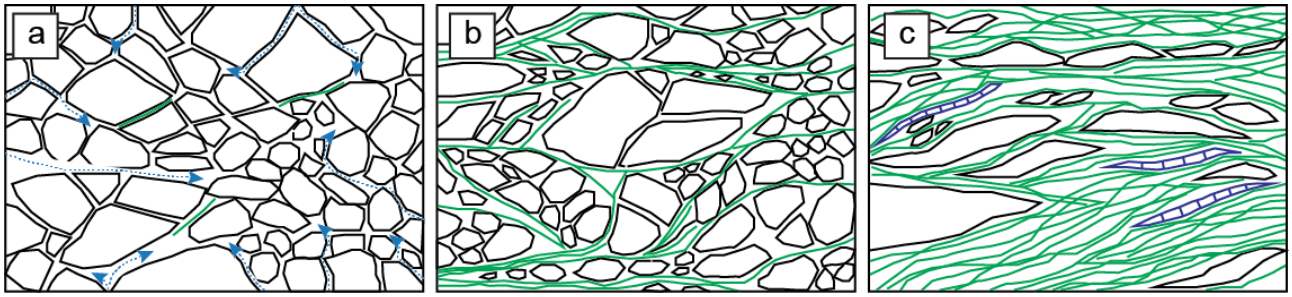

Figure 8. Schematic representation of reaction softening with increasing strain. a) At the onset of deformation fracturing associated to cataclasis increases permeability favouring the influx of fluids (blue arrows) into the fault zone. b) Fluids react with the fine-grained cataclasite promoting dissolution of the strong granular phases and precipitation of phyllosilicates (green lines). c) At high strains the microstructure consists of an interconnected phyllosilicate-rich network where the deformation is predominantly accommodated by frictional sliding along the (001) phyllosilicate lamellae. The phyllosilicate network is also a low-permeability horizon for transversal fluid flow favouring the development of fluid overpressure testified by foliation parallel veins with crack-and-seal texture (dark-blue). Key-references on the processes highlighted in this picture are reported on the main text.

Within the fault zone, from early to mature stages of deformation, there is an evolution from a granular load-bearing network to a weak and interconnected foliated microstructure (e.g. Handy, 1990; Holdsworth, 2004). A similar microstructural evolution involving the combined effect of pressure solution of granular materials and frictional sliding on phyllosilicates have been reproduced in the laboratory, mainly at Utrecht University (e.g. Bos & Spiers 2001). The associated mechanical data have been used to characterize a frictional-viscous behavior (i.e., both normal stress and strain rate dependent) active within the seismogenic crust and describe its implications for crustal strength profiles (Bos & Spiers 2001; Niemeijer & Spiers, 2005; Den Hartog and Spiers, 2014). The rheological strength profiles for a foliated and phyllosilicate-rich faults contained within the seismogenic crust is composed of three main deformation regimes (Fig. 9): A) at shallow crustal level, the deformation is mainly accommodated by cataclastic processes involving dilation: this behaviour closely resembles the Byerlee's rule with a linear trend controlled by high (μ = 0.6-0.85) friction; C) at greater depth, following the development of interconnected phyllosilicate-rich networks via pressure-solution processes, the slip behaviour is mainly controlled by frictional sliding along the phyllosilicate foliae, i.e. linear trend with low friction (cf. paragraph 3.3 for details on friction); B) the transition region represents the pressure solution controlled regime (regime B), where mechanical behavior is strongly rate-sensitive as well as normal stress sensitive. At larger crustal depth, frictional sliding along the phyllosilicates (regime C) is replaced by plastic flow.

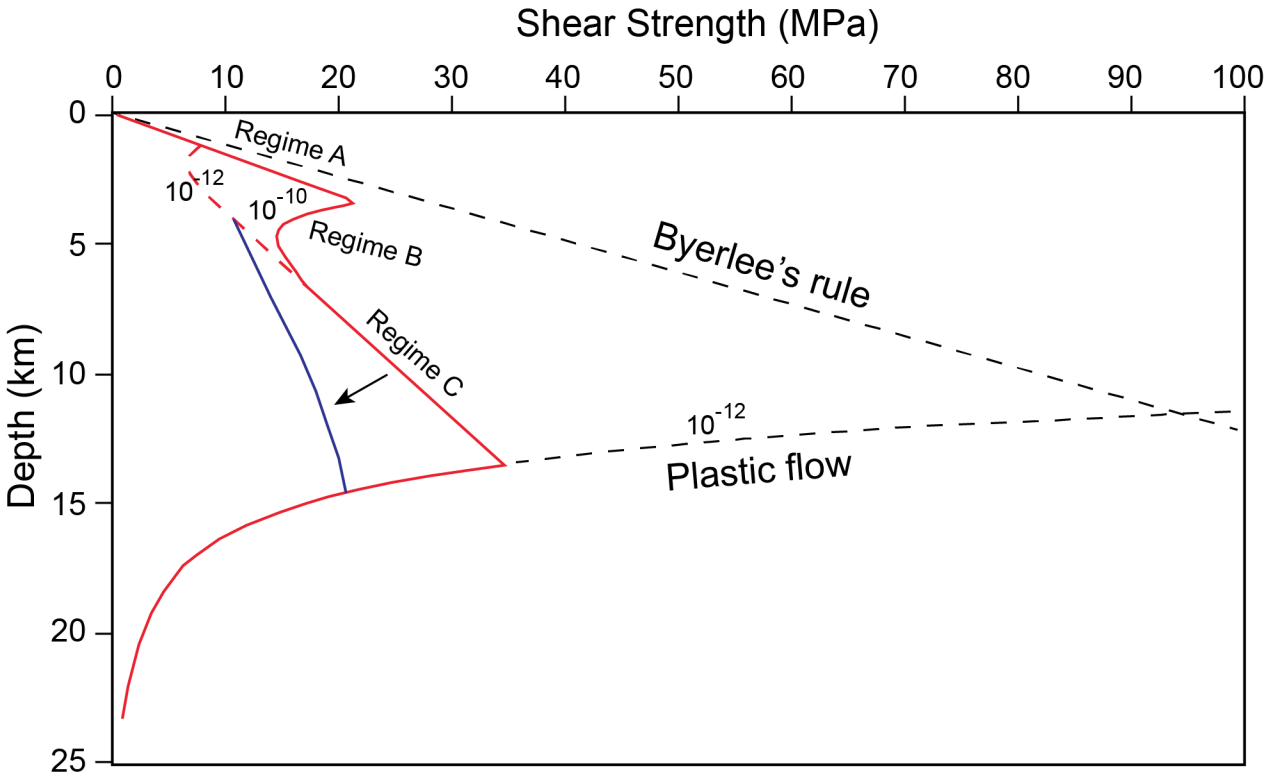

Figure 9. Crustal strength profile for a quartz (Byerlee's friction) muscovite (μ = 0.3) assemblage within a strike-slip fault (from Niemeijer and Spiers, 2005). The model of Niemeijer and Spiers (red curve) defines three main deformation regimes in which the strength is dominated by: A) cataclastic deformation; B) pressure solution; C) frictional sliding on phyllosilicate foliae. With increasing crustal depth frictional sliding along the phyllosilicates is replaced by crystal-plastic flow of quartz. The strength profile is constructed for a geothermal gradient of 25°C/km and the influence of strain rate on the depth of pressure solution accommodated deformation (regime B) is shown for strain-rates of 10^{-10} and 10^{-12} s^{-1}. Reduction in phyllosilicate-friction or the onset of phyllosilicate plasticity for high geothermal gradients (e.g. Wallis et al., 2015) can promote further strength reduction (blue curve).

3.3 Frictional properties of phyllosilicate-rich faults

The simple conceptual model we can reconstruct by merging the observations presented in paragraphs 3.1 and 3.2 suggests that fluid-rock interaction within fault zones might produce frictional-viscous flow with the development of interconnected networks of phyllosilicates resulting in fault weakness. In regime C, the low-strength of the fault is mainly controlled by frictional sliding along phyllosilicate foliae. To provide mechanical evidence for this weakness, here we present a vast compilation of frictional measurements on phyllosilicate-rich faults.

Data reported here have been collected during friction experiments at low sliding velocities, in general 0.01- 100 μm/s. These experiments are used as a proxy to evaluate the steady state frictional strength of a fault during the interseismic or pre-seismic phase of the seismic cycle.

To characterize the frictional properties of fault rocks during laboratory experiments a

constant normal stress is applied on the rock sample and then a shear stress is induced by shearing the fault at constant sliding velocity. The experimental fault generally shows an initial phase, where the shear stress increases rapidly during elastic loading, before a yield point, followed by shear at a steady-state friction value (Fig. 10a). During these friction experiments velocity steps and slide-hold-slide sequences are usually performed to characterize the frictional stability together with the healing properties of the tested material (e.g. Dieterich, 1979; Ruina, 1983; Marone 1998a and references therein).

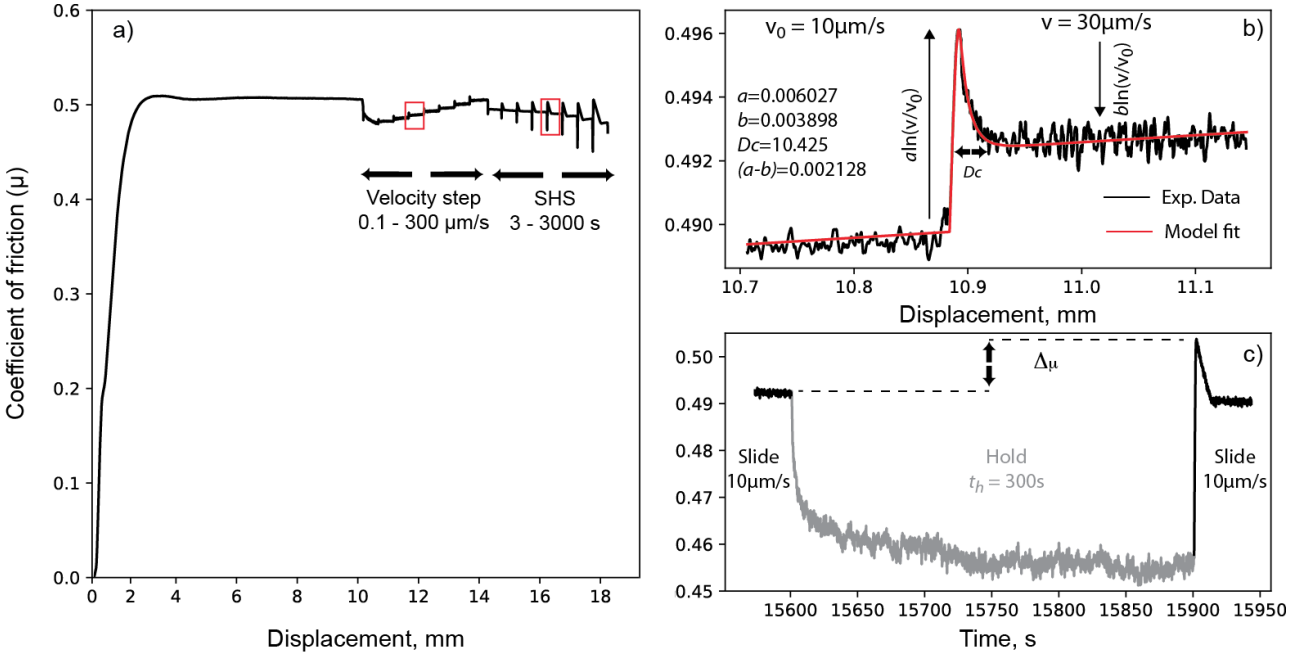

Figure 10. Laboratory experiment to characterize the rock frictional properties. The tested material is powdered illite at room humidity and room temperature. a) A typical experiment to characterize the frictional properties of a fault consists of a run-in phase to achieve steady state shear strength and measure steady state friction. Then velocity steps b) and/or c) slide-hold slide, SHS, tests are usually performed to constrain the velocity dependence of friction, *a-b*, the critical slip distance D_c, and the healing properties, Δ_μ, of the experimental fault.

During velocity-stepping tests (Fig. 10b) a near-instantaneous step change in sliding velocity from V_0 to V is imposed and the new sliding velocity is held constant until a new steady state shear stress level is attained. The instantaneous change in friction scales as the friction parameter $a\ln(V/V_0)$, where *a* is an empirical constant defined as the direct effect (e.g., Ruina, 1983). The subsequent drop to a new steady state value of friction scales as the friction parameter $b\ln(V/V_0)$, where b is an empirical constant defined as the evolution effect (e.g., Ruina, 1983). D_c is the critical slip distance that is the displacement over which the population of asperity contacts that control friction are renewed. The velocity dependence of steady state friction (*a* - *b*) is defined as:

$$(a-b) = \frac{\Delta\mu_s}{ln\left(V/V_0\right)} \quad (4)$$

where $\Delta\mu_s$ is the change in steady state friction. Positive values of (a - b), indicate velocity-strengthening behavior, that favours stable sliding and fault creep. Negative values of (a - b), represent a velocity-weakening behavior, that is a requirement for the nucleation of slip instability (e.g. Dieterich and Kilgore, 1994; Marone, 1998a; Scholz, 2002).

In slide-hold-slide tests (e.g., Dieterich and Kilgore, 1994; Marone, 1998b; Carpenter et al., 2016) slip at constant velocity is followed by a hold period, t_h, usually ranging from 1 to 3000 s, during which sliding is halted and subsequently resumed. The amount of frictional healing, $\Delta\mu$, is measured as the difference between the peak friction measured upon re-shear after each hold and the pre-hold steady state friction, μ_{ss} (Fig. 10c). Frictional healing rate β is calculated as:

$$\beta = \Delta\mu / \Delta\, log_{10}(t_h) \quad (5)$$

It is important to note that in the Byerlee's (1978) dataset, friction measurements on pure clays show values well below the range he proposed. However, since fault zones are not composed of a single mineral phase, it was not clear how the mixing of strong and weak phyllosilicates would have affected fault strength.

Fault weakness resulting from fluid-assisted reaction softening originates at the scale of individual mineral grains and the ability to transmit this local effect to crustal scale faults is due to the interconnectivity of the phyllosilicate-rich networks. In other words, even a low percentage of weak mineral phases can induce significant fault weakening if the interconnectivity of the weak minerals is very high (Niemeijer et al., 2010). In order to capture the role of phyllosilicate interconnectivity in frictional properties of weak faults, instead of running traditional friction experiments on powdered fault rocks or on bare rock surfaces, we collected large blocks of foliated natural fault rocks and we cut them to form wafers 0.8–1.2 cm thick and 5 cm x 5 cm in area. This approach is akin to the one used to constrain the role of anisotropy in the strength of foliated metamorphic rocks (e.g. Shea and Kronenberg, 1993). The wafers were oriented so that they could be sheared in their in situ orientation, with foliation parallel to shear direction (e.g. Collettini et al., 2009b). We refer these as wafer experiments and microstructural analyses of these sheared samples show that:

a) the original foliated microstructure is preserved and 2) most of the deformation occurs by frictional sliding along the phyllosilicate-rich network with very limited cataclasis and grain-size reduction (Collettini et al., 2009b; Tesei et al., 2014; 2015; Smith et al., 2017). Other laboratory experiments on powdered fault rocks mixing different percentages of weak and strong mineral phases have documented a decrease in frictional strength with the addition of weak phases (Logan and Rauenzahn, 1987; Saffer and Marone, 2003; Takahashi et al., 2007; Crawford et al., 2008; Giorgetti et al., 2015). In particular an amount of weak phases greater than 40-50% of the rock volume results in significant fault weakness because it is sufficient to promote interconnectivity of the weak mineral phase through the entire experimental fault. This implies that when the weak mineral phases are abundant, laboratory experiments on powdered materials are similar to those conducted on wafers.

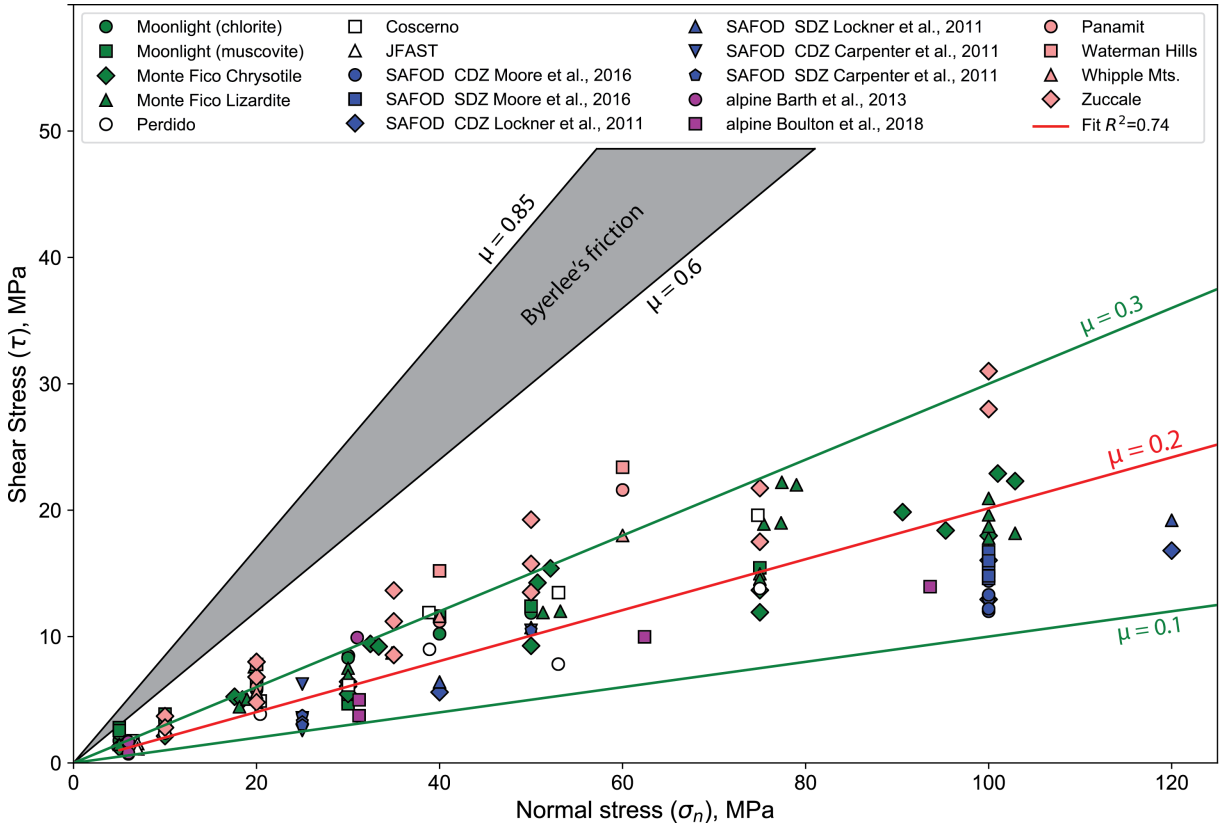

Figure 11. Frictional properties of phyllosilicate-rich faults. The dataset together with key references is summarized in Table 2.

Figure 11 shows normal stress vs. steady state shear stress from friction tests conducted on a large number of natural fault rocks rich in phyllosilicates, both wafers or powdered material with phyllosilicates percentages > 40%, under a wide range of experimental conditions (the dataset together with key references is summarized in Table 2). Each rock type plots along a

line consistent with a brittle failure envelope and the frictional strength of all the tested materials is significantly below the Byerlee range. The average friction for all the tested material is 0.2 and at first approximation it is not influenced by the applied normal stress and temperature. The highest friction values, $0.25 < \mu_s < 0.43$ (pink colour in figure 11), are recorded for dry experiments on fault rocks from US detachment and from the Zuccale fault. These fault rocks are rich in clays and further weakening for these minerals is expected in the presence of water (Moore and Lockner, 2004, 2007). The tested phyllosilicate-rich fault rocks are characterized by a velocity strengthening behaviour, i.e. by positive *(a-b)*, which in general becomes more pronounced with increasing sliding velocity (Fig. 12a). Limited velocity weakening is reported systematically for the Southern Deforming Zone, SDZ, of the San Andreas at SAFOD for temperatures above 200 °C (Moore et al., 2016). The phyllosilicate-rich fault rocks also show near zero or limited healing rates, $-0.0023 < \beta < 0.003$ (Fig. 12b), that is significantly lower in comparison to granular materials such as quartz, $0.0082 < \beta < 0.0086$ (Marone, 1998b), quartz-feldspatic rocks $0.007 < \beta < 0.008$ (Carpenter et al., 2016) and calcite, $0.015 < \beta < 0.03$ (Carpenter et al., 2014).

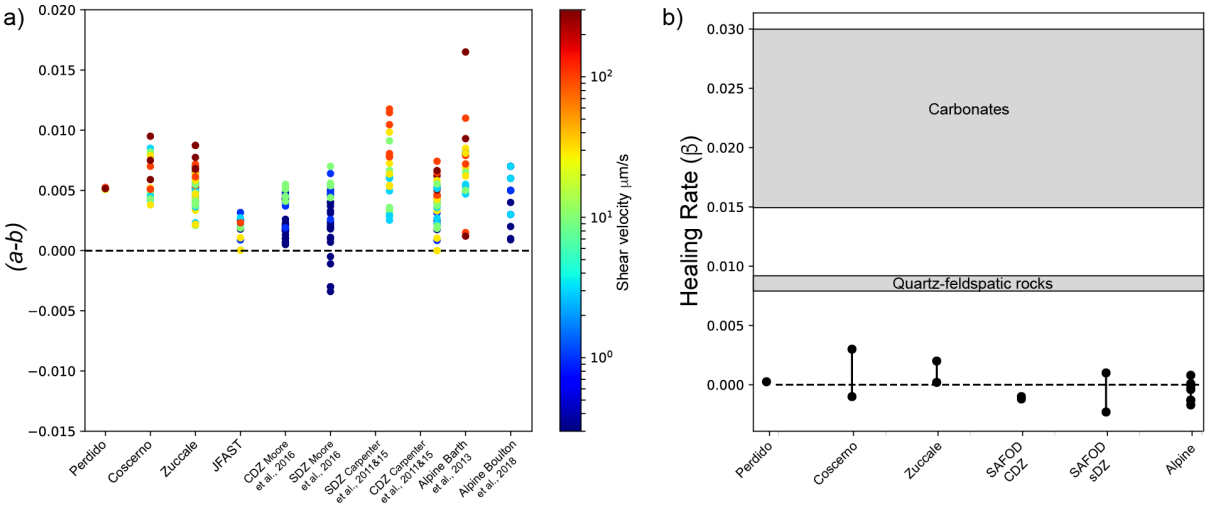

Figure 12. a) Velocity dependence of friction of phyllosilicate-rich faults. b) Healing properties of phyllosilicate-rich faults and comparison with quartz-feldspatic (Marone, 1998b; Carpenter et al., 2016) and calcite-rich (Carpenter et al., 2014) rocks. The dataset together with key references is summarized in Table 2.

4. Discussion

4.1 Structural and frictional heterogeneous crustal faults

In this review we have documented (via outcrops, microstructural and laboratory data) several examples of crustal faults characterized by either high (paragraph 2) or low (paragraph 3) strength. When considered all together these data point to the heterogeneous structural nature of crustal scale faults. In particular, a single crustal scale fault, tens of

644 kilometres long, can be characterized by weak fault patches in zones where crustal fluids
645 exerted a chemical role, facilitating the replacement of strong with weak mineral phases, and
646 strong fault patches, where fluid-assisted reaction softening were not efficient, and crustal
647 deformation was achieved predominantly by fragmentation, grain-size reduction and
648 localization (Fig. 13). Similar heterogeneities have been documented on the grounds of
649 frequency content of seismic waveforms of large and great earthquakes on subduction zone
650 megathrusts (e.g. Lay et al., 2012), from high-resolution spatio-temporal behaviour of
651 seismicity (e.g. Rubin et al., 1999; Waldhauser et al., 2004; Chiaraluce et al., 2007), and from
652 geodetic imaging of active faults (e.g. Avouac, 2015 and references therein).
653
654 Strong faults or strong fault portions like those described in paragraph 2.3 (Fig. 13) form
655 predominantly when granular mineral phases like quartz, feldspar, pyroxene, olivine, calcite
656 and dolomite are dominant and repeated fault reactivation during the geologic fault history
657 allows the development of fault rocks like gouge or cataclasite. The similarities in the internal
658 structure of experimental and natural faults point to similarities in the deformation
659 mechanism (Tchalenko, 1970). Large-displacement natural faults in granular materials show
660 the evidence of localization along fault-parallel principal slip zones that are present at all
661 depths through the seismogenic crust (Chester and Chester 1998; Sibson, 2003). Similarly,
662 experimental faults show that at high-strains the deformation is accommodated along distinct
663 fault-parallel shear zones, showing intense grain-size reduction (Logan et al., 1979; Beeler et
664 al., 1996; Scuderi et al., 2017). Collectively these faults are characterized by a granular load-
665 bearing microstructure with a frictional strength controlled by Byerlee's rule (e.g. Weeks and
666 Tullis, 1985; Biegel et al., 1989; Marone, 1998a; Beeler et al., 1996; Verberne et al., 2010;
667 Scuderi et al., 2013; Carpenter et al., 2014). With increasing strain, localization along a
668 principal slip zone promotes the passage from rate strengthening to rate weakening
669 behaviour (Beeler et al., 1996; Ikari et al., 2011; Scuderi et al., 2017) favouring the occurrence
670 of a frictional instability. Frictional instabilities and associated earthquake slip along strong
671 faults is documented by extreme localization, < 1 cm (e.g. Chester and Chester, 1998), and by
672 the presence within the principal slip zone of fault rocks such as pseudotachylites, amorphous
673 silica, polygonal nano-grains and decomposed minerals, produced by intense frictional
674 heating during earthquake slip (paragraph 2.3 and Rowe and Griffith, 2014 for a
675 comprehensive review). Following the earthquake, the fault regains strength during the
676 interseismic period because in the fault zone the increase in grain contact quantity and
677 quality promotes significant fault healing (Marone 1998b; Carpenter et al., 2014). Further re-

678 strengthening is also achieved via sealing and cementation processes (e.g. Sibson, 1992;
679 Tenthorey et al., 2003).
680
681 Weak faults or weak fault patches result from fluid-assisted fault weakening (e.g. paragraph
682 3.2) that, during the long-term evolution of the fault, might promote the replacement of strong
683 minerals (quartz, feldspar, olivine, pyroxene, calcite, dolomite) with weak phyllosilicates.
684 Fluid flow into the fault zone is controlled by fracturing and therefore mineral replacement is
685 a pervasive process within the fault core and the damage zone (Caine et al., 1996), and results
686 in interconnected networks of weak phyllosilicates (Fig. 13).
687 The development of phyllosilicate networks formed via fluid-assisted reaction softening has
688 been documented at different crustal depths, from shallow to deep crust, in different tectonic
689 regimes and from different protoliths such as carbonates, dolostones, marly-carbonates,
690 sandstones, ultramafic rocks and quartz-feldspatic dominated lithologies (paragraph 3.2 and
691 table 1). Therefore, fluid-assisted reaction softening and associated frictional-viscous
692 behavior can be considered as a general weakening mechanism within the seismogenic crust.
693 The weakness resulting from frictional-viscous behaviour originates at the scale of individual
694 mineral grains and the ability to transmit this local effect to crustal scale faults is due to the
695 interconnectivity of the phyllosilicate-rich networks (e.g. Handy, 1990; Holdsworth, 2004;
696 Collettini et al., 2009b). In laboratory experiments the low frictional strength of phyllosilicate-
697 rich faults (Fig. 11), despite the fact that in some cases phyllosilicates are present in relatively
698 small quantities, is mainly due to the interconnectivity of phyllosilicates and frictional sliding
699 along the phyllosilicate foliae with very limited cataclastic processes (Fig. 13 green parts and
700 details in Collettini et al., 2009b, Tesei et al., 2015). Friction measurements on these
701 phyllosilicate-rich natural fault rocks show that friction is significantly below Byerlee's range
702 and extends from $0.1 < \mu_s < 0.3$ (Fig. 11 and table 2). Frictional sliding along phyllosilicates-
703 rich faults acts in concert with dissolution and precipitation processes (Niemeijer and Spiers,
704 2005; Gratier et al., 2011; Fagereng and den Hartog 2016), and in some cases dissolution
705 accommodated deformation is so fast that it does not contribute to strength (e.g. regime 3 in
706 Fig. 9). Frictional sliding along the phyllosilicate foliae (Fig. 13) is a sliding mechanism by
707 which mineral surfaces tend to remain in complete contact and thus the real contact area does
708 not evolve during the velocity steps or during the hold periods. The concept of contact
709 saturation has been proposed as reasonable explanation for: a) the low *b* values during the
710 velocity steps, promoting the velocity strengthening behaviour (Fig. 12a and Saffer and
711 Marone, 2003; Ikari et al., 2009); and b) the absence of contact growth during the hold

712 periods resulting in null healing rates (Fig. 12b and Carpenter et al., 2011; Tesei et al., 2012).
713 Moreover, phyllosilicate coating strongly hinders rock cementation (Dewers and Ortoleva,
714 1991; Worden and Morad, 2000), which together with null frictional healing suggests the
715 inability of these fault zones to store elevated elastic stress. Collectively, these frictional
716 properties indicate that foliated, phyllosilicate-rich faults are weak, they accommodate
717 deformation predominantly by aseismic creep, or to be more precise (see discussion below) a
718 seismic rupture nucleation is inhibited within these lithologies, and remain weak over long
719 time scales.
720
721 Our conceptual model of heterogeneous fault zone structures builds on the documented fluid-
722 assisted reaction softening (paragraph 3) and on measured frictional properties of the
723 resulting natural fault rocks. The model indicates that single faults might be characterized by
724 strong and weak fault patches (Fig. 13). Further weakening, not considered in the conceptual
725 model, is due to fluid pressure development during the fault activity related to the spatial and
726 temporal variability of fault zone permeability (e.g. Cox, 1995; Miller et al., 1996; Faulkner et
727 al., 2010; Sibson, 2017). For example, the development of continuous and phyllosilicate-rich
728 networks strongly reduces fault permeability (Faulkner and Rutter, 2001; Ikari et al., 2009)
729 facilitating the entrapment of crustal fluids deriving from various sources, e.g. meteoric fluids,
730 mantle degassing, metamorphic reactions. Fluid pressure build-up and release during the
731 deformation of phyllosilicate-rich faults is testified by the numerous hydrofracture systems
732 contained within these shear zones (e.g. figure 4c, 5b, 7b and details in Chester et al., 1993;
733 Imber et al., 1997; Collettini et al., 2006; Fagereng and Sibson, 2010; Sibson, 2017).
734

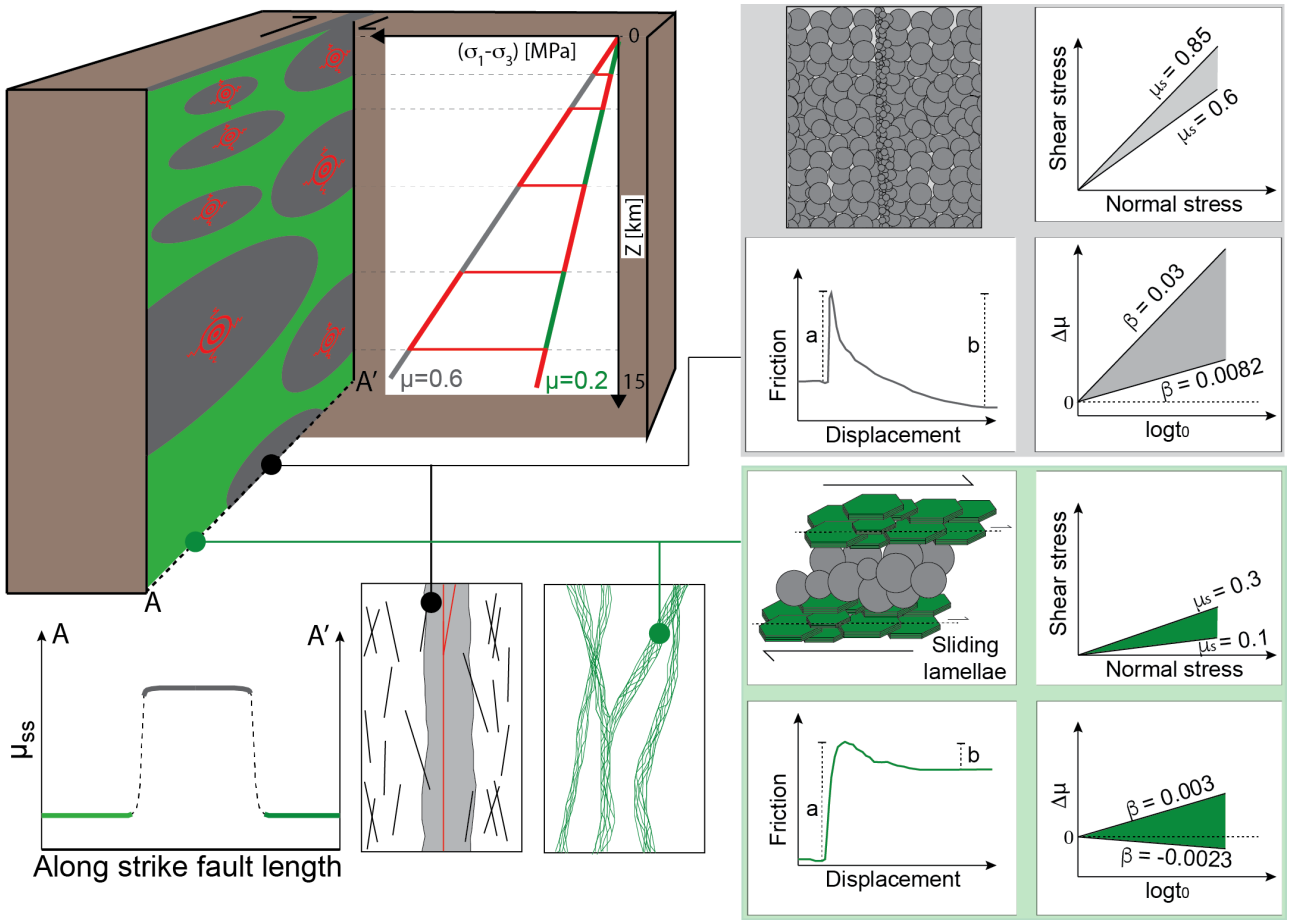

Figure 13. An integrated view of the internal structure and mechanical properties of heterogeneous faults. Schematic cross-section with strong (grey) and weak (green) fault portions (top-left). Steady state frictional strength profile along a vertical (red path) and sub-horizontal transect (A-A' bottom left). The strong portion (grey drawings and data) is mainly characterized by granular mineral phases affected by cataclasis and grain-size reduction with localization along a principal slipping zone (red-line), usually < 1 cm in thickness. This is associated to Byerlee friction, a velocity weakening behaviour, i.e. negative *(a-b)*, and high healing rates, β. In the weak fault portions (green drawings and data), distributed deformation occurs along interconnected phyllosilicate-rich networks and frictional sliding along phyllosilicate lamellae favours low friction, $0.1 < \mu_s < 0.3$, velocity strengthening, i.e. positive *(a-b)*, and very low healing rates.

4.2 Fault patches interaction during tectonic loading

During tectonic loading, weak and velocity-strengthening phyllosilicate-rich patches slip aseismically (Fig. 13 green parts). Creep along weak patches, facilitated also by pressure solution processes (e.g. Gratier et al., 2011; 2013; Fagereng and Den Hartog, 2016), allows for stress build up in the surrounding strong patches that during the interseismic phase remain locked due to high strength and healing rates (Fig. 13 grey parts). Analyses based on the assumption of stress and strain continuity across the weak-strong interface, and the

observation that more strain is accommodated in the phyllosilicate-rich networks, support the idea of stress concentration in the strong lenses (e.g. Fagereng and Sibson, 2010; Fagereng and Den Hartog, 2016). When the shear stress overcomes the frictional strength of the strong, velocity-weakening patch an earthquake rupture might nucleate. In particular, frictional stick-slip instabilities occur when the fault-weakening rate with slip exceeds the maximum rate of elastic unloading, resulting in a force imbalance and fault acceleration (e.g., Scholz, 2002). If the condition to nucleate an earthquake instability is satisfied, the extent of the rupture will be controlled by the distribution and dimensions of velocity weakening vs. velocity strengthening fault patches, their state of stress, and the energy dissipated as seismic slip propagates (e.g. Boatwright and Cocco, 1996; Kaneko et al., 2010; Faulkner et al., 2011; Noda and Lapusta 2013; Avouac, 2015). Numerical models, reproducing the rich earthquake slip behaviours similar to that of natural faults, show that velocity strengthening fault patches tend to inhibit rupture propagation and the probability for a seismic rupture to propagate through a velocity-strengthening patch is related to the dimension and the frictional properties of the patch itself (Kaneko et al., 2010). However high-velocity friction experiments have shown that wet clay at low slip velocity is velocity strengthening, but at high slip velocity it weakens immediately or remains weak resulting in negligible fracture energy, making rupture propagation through clay-rich fault portions energetically very favourable (Faulkner et al., 2011). These experimental findings have been incorporated in numerical models and it has been shown that stable velocity strengthening segments may host seismic ruptures as result of mechanisms such as dynamic weakening (Noda and Lapusta, 2013). The transition from velocity strengthening at low sliding velocities (0.1-300 μm/s) to slip dominated by dynamic weakening approaching seismic slip rates (tens of cm per seconds) have been invoked (Wibberley et al., 2008; Faulkner et al., 2011; Noda and Lapusta, 2013) to explain the exceptionally large seismic slip, of as much as 50 m (Ide et al., 2011), in the shallower area of the Mw 9.0 Tohoku-Oki earthquake, where clay rich materials are present (Kameda et al., 2015).

Our conceptual model for the slip behaviour of heterogeneous faults (Fig. 13) agrees with the increasing number of geodetic observations showing that in the interseismic period some fault areas remain locked whereas others creep aseismically (e.g. Avouac 2015 and references therein). The model is also consistent with the analysis of the stress orientations in subduction zones suggesting that creeping subduction zones are weaker than locked ones (Hardebeck and Loveless, 2018). However, another source of structural heterogeneities, that is likely to play a key-role on fault slip behaviour and not considered in our simplified

conceptual model, is due to fault roughness. For example in areas of extremely rugged subducting seafloor, creeping is the predominant mode of subduction (e.g. Wang and Bilek, 2014, but see also Scholz and Small, 1997 for a different interpretation) whereas mega-earthquakes rupture seems to be more likely along flat portions of the megathrust because the shear strength is more homogeneous, and hence more likely to be exceeded simultaneously over large areas (Bletery et al., 2016). Laser-based methods to map exposed fault surfaces have shown that large-slip faults are polished at small scales but contain elongated quasi-elliptical bumps and depressions at scales of a few to several meters (Renard et al., 2006; Sagy et al., 2007; Brodsky et al., 2011). This difference in geometry play an important role in the nucleation, growth, and termination of earthquakes (Sagy et al., 2007).

4.3 Some challenging topics

While there is an increasing amount of geological evidence that relates the occurrence of seismic ruptures within strong fault patches (some details and references in paragraph 2.3 and Rowe and Griffith, 2014 for an extensive review), clear geological evidence of rupture propagation through weak and velocity strengthening phyllosilicate fault patches at depth is rare. Recently Tarling et al., (2018) showed that within a tens to several hundreds of metres wide serpentinite shear zone, where the bulk deformation is accommodated by dissolution and precipitation processes plus frictional sliding along lizardite and fibrous chrysotile (i.e. processes indicative of aseismic creep) polished and localized fault surfaces in magnetite-rich patches contain high temperature reaction products, in the form of nanocrystalline olivine and enstatite, that likely formed during earthquake rupture propagation through the creeping serpentinites. Similar examples can be represented by the narrow and clay-rich slip zone within the Median Tectonic Line in Japan (Wibberley and Shimamoto, 2003) or by the pseudotachylyte-bearing fault rocks contained within the foliated argillaceous matrix of the Pasagshak Point thrust in Alaska (Rowe et al., 2011). On this research line, more field studies are required to better document the occurrence of seismic rupture propagation within rate-strengthening fault rocks. Furthermore, future laboratory tests should aim at reproducing experimental faults composed of both rate-strengthening and rate-weakening fault patches (e.g. Corbi et al., 2017 in rock analogues) to better illuminate the interaction between weak and strong fault patches.

The observations on fault zone structure and frictional processes presented here suggest that fault creep and slow slip might play an important role in the earthquake preparatory phase. Although distinguishing the processes operating during the earthquake nucleation still

remains a great challenge (e.g. Gomberg et al., 2018) and some earthquakes show no evidence of aseismic slip in the earthquake preparatory phase, at least in the absence of measurements in the near field of the hypocentre (Ellsworth and Bulut, 2018), other evidences suggest the presence of slow-slip phenomena in or nearby the fault patch hosting the future mainshock. The foreshock activity of the Mw 9.0 Tohoku-Oki earthquake indicates that two sequences of slow slip transients propagated toward the initial rupture point of the earthquake (Kato et al., 2012). For the Mw 8.1 Iquique earthquake, more than 1 m of aseismic slip has been documented in the 15 days preceeding the event, in the same area where the mainshock occurred (Ruiz et al., 2014). High-resolution seismological data have shown that an Mw 3.7 earthquake in Alaska was preceded by a slow slip phase that accelerates into a fast rupture (Tape et al., 2018). Fluid injection experiments on laboratory and natural faults reveal a similar phase of sustained aseismic creep that increases shear stress beyond the pressure front and promote earthquake triggering (Cappa et al., 2019). Collectively, these observations significantly renew the interest in precursory signals and although the detection of reliable earthquake precursors remains an open issue, now there is some cause for optimism. The structural and frictional heterogeneous nature of crustal faults presented in this manuscript suggests that creep and slow slip play a fundamental role in the deformation of crustal faults including the earthquake preparatory phase. Preparatory processes such as slow slip and seismicity migration before large earthquakes can be monitored with a combination of seismic and geodetic observations, and the physics of these processes can be constrained by structural geology and laboratory experiments, and implemented in numerical models. Innovative and original data sets will be needed to establish whether and if the observation of such signals before the mainshocks repeats in time, then leading to a reliable contribution to the forecast.

Acknowledgements

A large amount of the dataset presented in the manuscript has been gathered to be presented at the 2018 Gordon Research Conference in Rock Deformation; we thank the organizers Julie Morgan and Dan Faulkner who gave us this opportunity. We thank everybody who provided helpful discussions during the preparation of this work, including Pablo Ampuero, Massimiliano Barchi, Nicola De Paola, Dan Faulkner, Carolina Giorgetti, Bob Holdsworth, Yoshi Kaneko, Matt Ikari, Chris Marone, André Niemeijer, Rick Sibson, Steve Smith. We also thank Chris Wibberley and an anonymous reviewer for very constructive comments.

References

Alder, S., Smith, S.A.F., Scott, J.M., 2016. Fault-zone structure and weakening processes in basin-scale reverse faults: the Moonlight Fault Zone, South Island, New Zealand. J. Struct. Geol. 91, 177–194.

Anderson E M 1905. The Dynamics of Faulting . Transactions of the Edinburgh Geological Society 8, 387-402, 1905, https://doi.org/10.1144/transed.8.3.387.

Anderson, E.M., 1951. The Dynamics of Faulting and Dyke Formation with Applications to Britain. Edinburgh, Oliver and Boyd, 206 p.

Avouac, J.P., 2015. From Geodetic Imaging of Seismic and Aseismic Fault Slip to Dynamic Modeling of the Seismic Cycle. Annu. Rev. Earth Planet. Sci. 2015.43:233-271, doi: 10.1146/annurev-earth-060614-105302.

Barth, N.C., Boulton, C.J., Carpenter, B.M., Batt, G.E., Toy, V.G., 2013. Slip localization on the southern Alpine Fault, New Zealand, Tectonics, 32, 620–640, doi:10.1002/tect.20041.

Beeler, N., Tullis, T., Blanpied, M.L., Weeks, J.D., 1996. Frictional behavior of large displacement experimental faults. Journal of Geophysical Research 101, 8697–8715, doi: 10.1029/96JB00411.

Ben-Zion, Y., Sammis, C.G., 2003. Characterization of fault zones. PAGEOPHP 160, 677–715.

Berthé, D., Choukroune, P., Jegouzo, P., 1979. Orthogneiss, mylonite and non coaxial deformation of granites: the example of the South Amorican Shear Zone. Journal of Structural Geology 1, 31-42, http://dx.doi.org/10.1016/0191-8141(79) 90019-1.

Biegel, R.L., Sammis, C.G., Dieterich, J.H., 1989. The frictional properties of a simulated gouge with a fractal particle distribution. J. Struct. Geol. 11, 827–46.

Bletery, Q., Thomas, A.M., Rempel, A.W., Karlstrom, L., Sladen, A., De Barros, L. 2016. Mega-earthquakes rupture flat megathrusts. Science 354, 1027–1031.

Boatwright, J., Cocco, M., 1996. Frictional constraints on crustal faulting. J. Geophys. Res. 101, 13895.

Bos, B., Spiers, C.J., 2001. Experimental investigation into the microstructural and mechanical evolution of phyllosilicate-bearing fault rock under conditions favouring pressure-solution. Journal of Structural Geology 23, 1187e1202. http://dx.doi.org/10.1016/S0191 8141(00)00184-X.

Boulton, C.J., Barth, N.C., Moore, D.E., Lockner, D.A., Townend, J., Faulkner, D.R., 2018. Frictional properties and 3-D stress analysis of the southern Alpine Fault, New Zealand. Journal of Structural Geology 114, 43–54.

Brodsky, E.E., Gilchrist, J.J., Sagy, A., Collettini, C., 2011. Faults smooth gradually as a function of slip. Earth and Planetary Science Letters 302, 185–193.

907 Bruhn, R., Parry, W.T.P., Yonkee, W.A., Thompson, T., 1994. Fracturing and Hydrothermal
908 Alteration in Normal Fault Zones. PAGEOPH 142, 609-644.
909
910 Bullock, R.J., De Paola, N., Holdsworth, R.E., Trabucho-Alexandre, J., 2014. Lithological controls
911 on the deformation mechanisms operating within carbonate-hosted faults during the seismic
912 cycle. Journal of Structural Geology 58, 22-42, http://dx.doi.org/10.1016/j.jsg.2013.10.0 08.
913
914 Bürgmann, R., 2018. The geophysics, geology and mechanics of slow fault slip. Earth and
915 Planetary Science Letters 495, 112–134, doi.org/10.1016/j.epsl.2018.04.062.
916
917 Byerlee, J., 1978. Friction of rocks. PAGEOPH 116, 615-626.
918
919 Byrne, D.E., Davis, D.M., Sykes, L.R., 1988. Loci and maximum size of thrust earthquakes and
920 the mechanics of the shallow region of subduction zones. Tectonics 7, 833–857,
921 doi:10.1029/TC007i004p00833.
922
923 Caine, J.S., Evans, J.P., Forster, C.B., 1996. Fault zone architecture and permeability structure.
924 Geology 24 (11), 1025-1028.
925
926 Carpenter, B.M., Marone, C., Saffer, D.M., 2011. Weakness of the San Andreas Fault revealed by
927 samples from the active fault zone. Nature Geoscience, 4, 251–254, doi:10.1038/NGEO1089.
928
929 Carpenter, B. M., Scuderi, M.M., Collettini, C., Marone, C., 2014. Frictional heterogeneities on
930 carbonate-bearing normal faults: Insights from the Monte Maggio Fault, Italy. J. Geophys. Res.
931 Solid Earth 119, 9062–9076, doi:10.1002/2014JB011337.
932
933 Carpenter, B. M., Saffer, D.M., Marone, C., 2015. Frictional properties of the active San Andreas
934 fault at SAFOD: Implications for fault strength and slip behavior. J. Geophys. Res. Solid Earth,
935 120, 5273–5289, doi:10.1002/2015JB011963.
936
937 Carpenter, B. M., Ikari, M.J., Marone, C., 2016. Laboratory observations of time-dependent
938 frictional strengthening and stress relaxation in natural and synthetic fault gouges, J. Geophys.
939 Res. Solid Earth, 121, 1183–1201, doi:10.1002/ 2015JB012136.
940
941 Chen, J., Niemeijer, A.R., Spiers, C.J., 2017. Microphysically Derived Expressions for Rate-and-
942 State Friction Parameters, a, b, and Dc. Journal of Geophysical Research,
943 https://doi.org/10.1002/2017JB014226.
944
945 Chester, F.M., Chester, J.S., 1988. Ultracataclasite structure and friction processes of the
946 Punchbowl fault, San Andreas system, California. Tectonophysics 295, 199–221.
947
948 Chester, F.M., Evans, J.P., Biegel, R.L., 1993. Internal structure and weakening mechanisms of
949 the San-Andreas fault. Journal of Geophysical Research e Solid Earth 98 (B1), 771-786.
950
951 Chester, J.S., Chester, F.M., Kronenberg, A.K., 2005. Fracture surface energy of the Punchbowl
952 fault, San Andreas system. Nature 437 (7055), 133-136.
953
954 Chiaraluce, L., Chiarabba, C., Collettini, C., Piccinini, D., Cocco, M., 2007. Architecture and
955 mechanics of an active low-angle normal fault: Alto Tiberina Fault, northern Apennines, Italy.
956 J. Geophys. Res., 112, B10310, doi:10.1029/2007JB005015.

957
958 Chiaraluce, L., 2012. Unravelling the complexity of Apenninic extensional fault systems: A
959 review of the 2009 L'Aquila earthquake (central Apennines, Italy). J. Structural Geoogy 42, 2–
960 18.
961
962 Chiaraluce, L., et al., 2017. The 2016 Central Italy seismic sequence: A first look at the
963 Mainshocks, aftershocks, and source models. Seismol. Res. Lett., doi:10.1785/0220160221.
964
965 Cloos, M., Shreve, R.L., 1988. Subduction-channel model of prism accretion, melange
966 formation, sediment subduction, and subduction erosion at convergent plate margins: 1.
967 Background and description. PAGEOPH, 128, 455–500.
968
969 Collettini, C., Sibson, R.H., 2001. Normal faults normal friction? Geology 29, 927–930.
970
971 Collettini, C., Holdsworth, R.E., 2004. Fault zone weakening processes along low-angle normal
972 faults: insights from the Zuccale Fault, Isle of Elba, Italy. J. Geol. Soc. 161, 1039–1051.
973
974 Collettini, C., De Paola, N., Goulty, N.L., 2006. Switches in the minimum compressive stress
975 direction induced by overpressure beneath a low-permeability fault zone. Terra Nova 18,
976 224-231, doi: 10.1111/j.1365-3121.2006.00683.x.
977
978 Collettini, C., De Paola, N., Faulkner, D.R., 2009a. Insights on the mechanics of the Umbria–
979 Marche earthquakes (Central Italy) from the integration of field and laboratory data:
980 Tectonophysics 476, 99–109, doi:10.1016/j.tecto.2008.08.013.
981
982 Collettini, C., Niemeijer, A., Viti, C., Marone, C.J., 2009b. Fault zone fabric and fault weakness.
983 Nature 462, 907–910.
984
985 Collettini, C., Viti, C., Smith, S.A.F., Holdsworth, R.E., 2009c. The development of inter-
986 connected talc networks and weakening of continental low-angle normal faults. Geology 37,
987 567–570.
988
989 Collettini, C., 2011. The mechanical paradox of low-angle normal faults: Current
990 understanding and open questions. Tectonophysics 510, 253–268,
991 doi:10.1016/j.tecto.2011.07.015.
992
993 Collettini, C., Niemeijer, A., Viti, C., Smith, S.A.F., Marone, C., 2011. Fault structure, frictional
994 properties and mixed-mode fault slip behavior. Earth Planet. Sci. Lett. 311, 316–327.
995 http://dx.doi.org/10.1016/j.epsl.2011.09.020.
996
997 Collettini, C., Viti, C., Tesei, S., Mollo, S., 2013. Thermal decomposition along natural carbonate
998 faults during earthquakes: Geology 41, 927-930, doi:10.1130/G34421.
999
1000 Collettini, C., Carpenter, B.M., Viti, C., Cruciani, F., Mollto, S., Tesei, T., Trippetta, F., Valoroso, L.,
1001 Chiaraluce, L., 2014. Fault structure and slip localization in carbon- ate bearing normal faults:
1002 an example from the Northern Apennines of Italy. J. Struct. Geol. 67, 154–166.
1003 http://dx.doi.org/10.1016/j.jsg.2014.07.017.
1004

Corbi, F., Herrendörfer, R., Funiciello, F., van Dinther, Y., 2017. Controls of seismogenic zone width and subduction velocity on interplate seismicity: Insights from analog and numerical models. Geophysical Research Letters, https://doi.org/10.1002/2016GL072415.

Cowan, D.S., 1974. Deformation and metamorphism of the Franciscan subduction zone complex northwest of Pacheco Pass, California. Geol. Soc. Amer. Bull. 85, 1623–1634.

Cowan, D.S., Cladouhos, T.T., Morgan, J., 2003. Structural geology and kinematic history of rocks formed along low-angle normal faults, Death Valley, California. Geological Society of America Bulletin 115, 1230–1248.

Cox, S.F., 1995. Faulting processes at high fluid pressures: An example of fault valve behavior from the Wattle Gully Fault, Victoria, Australia. Journal of Geophysical Research https://doi.org/10.1029/95JB00915.

Craig, T.J., Copley, A., Middleton, T. A., 2014. Constraining fault friction in oceanic lithosphere using the dip angles of newly-formed faults at outer rises. Earth and Planetary Science Letters 392, 94–99, doi.org/10.1016/j.epsl.2014.02.024.

Crawford, B.R., Faulkner, D.R., Rutter, E. H., 2008. Strength, porosity, and permeability development during hydrostatic and shear loading of synthetic quartz-clay fault gouge. Journal of Geophysical Research, 113, B03207. https://doi.org/10.1029/2006JB004634.

Davis, D., Suppe, J., Dahlen, F.A., 1983. Mechanics of fold-and-thrust belts and accretionary wedges. Journal of Geophysical Research 88, B2, 1153–1172, doi:10.1029 /JB088iB02p01153.

De Paola, N., Collettini, C., Faulkner, D.R., Trippetta, F., 2008. Fault zone architecture and deformation processes within evaporitic rocks in the upper crust. Tectonics 27. http://dx.doi.org/10.1029/2007TC002230.

De Paola, N., Holdsworth, R.E., Viti, C., Collettini, C., Bullock, R., 2015. Can grain size sensitive flow lubricate faults during the initial stages of earthquake propagation? Earth Planet Sci. Lett. 431, 48–58. http://dx.doi.org/10.1016/j.epsl.2015.09.002.

Den Hartog, S., Spiers, C.J., 2014. A microphysical model for fault gouge friction applied to subduction megathrusts. J. Geophys. Res. 119, 1510–1529. http://dx.doi.org/10.1002/2013JB010580.

Dewers, T., Ortoleva, P., 1991. Influences of clay minerals on sandstone cementation and pressure solution. Geology 19, 1045-1048.

Di Toro, G., Pennacchioni, G., 2005. Fault plane processes and mesoscopic structure of a strong-type seismogenic fault in tonalites (Adamello batholith, Southern Alps). Tectonophysics 402, 55–80.

Di Toro, G., Han, R., Hirose, T., De Paola, N., Nielsen, S., Mizoguchi, K., Ferri, F., Cocco, M., Shimamoto, T., 2011. Fault lubrication during earthquakes. Nature 471 (7339), 494–498.

Dieterich, J.H., 1979. Modeling of rock friction 1. Experimental results and constitutive equations. J. Geophys. Res., Solid Earth 84, 2161–2168,

1055 http://dx.doi.org/10.1029/JB084iB05p02161.
1056
1057 Dieterich, J. H., Kilgore, B.D., 1994. Direct observation of frictional contacts: New insights for
1058 state-dependent properties, Pure Appl. Geophys.,143, 283–302, doi:10.1007/BF00874332.
1059
1060 Ellsworth, W.L., Bulut, F. 2018. Nucleation of the 1999 Izmit earthquake by a triggered
1061 cascade of foreshocks. Nat. Geosci. https://doi.org/10.1038/ s41561-018-0145-1 (2018).
1062
1063 Escartin, J., Hirth, G., Evans, B., 2001. Strength of slightly serpentinized peridotites:
1064 Implications for the tectonics of oceanic lithosphere. Geology 29, 1023–1026.
1065
1066 Evans, J.P., Chester, F.M., 1995. Fluid–rock interaction in faults of the San Andreas system:
1067 Inferences from San Gabriel fault rock geochemistry and microstructures. J. Geophys. Res.
1068 100, 13007–13020.
1069
1070 Fagereng, A., Cooper, A.F., 2010. The metamorphic history of rocks buried, accreted and
1071 exhumed in an accretionary prism: an example from the Otago Schist, New Zealand. J.
1072 Metamorph. Geol 28, 935–954.
1073
1074 Fagereng, A., Sibson, R.H., 2010. Melange rheology and seismic style. Geology 38, 751–754.
1075
1076 Fagereng, A., den Hartog, S.A.M., 2016. Subduction megathrust creep governed by pressure
1077 solution and frictional–viscous flow. Nature Geoscience DOI: 10.1038/NGEO2857.
1078
1079 Faulkner, D.R., Rutter, E.H., 2001. Can maintainance of overpressured fluids in large strike –
1080 slip fault zones explain their apparent weakness? Geology 29, 503–506.
1081
1082 Faulkner, D.R., Lewis, A.C., Rutter, E.H., 2003. On the internal structure and mechanics of large
1083 strike-slip fault zones: field observations of the Carboneras fault in southeaster Spain.
1084 Tectonophysics 367, 235-251.
1085
1086 Faulkner, D.R., Mitchell, T.M., Healy, D., Heap, M.J., 2006. Slip on 'weak' faults by the rotation of
1087 regional stress in the fracture damage zone. Nature 444, 922-925.
1088
1089 Faulkner, D.R., Jackson, C.A.L., Lunn, R.J., Schlische, R.W., Shipton, Z.K., Wibberley, C.A.J.,
1090 Withjack, M.O., 2010. A review of recent developments concerning the structure, mechanics
1091 and fluid flow properties of fault zones. J. Struct. Geol. 32, 1557–1575.
1092 http://dx.doi.org/10.1016/j.jsg.2010.06.009.
1093
1094 Faulkner, D.R., Mitchell, T.M., Behnsen, J., Hirose, T., Shimamoto, T., 2011. Stuck in the mud?
1095 Earthquake nucleation and propagation through accretionary forearcs. Geophys. Res. Lett. 38,
1096 L18303.
1097
1098 Fondriest, M., Smith, S.A.F., Candela, T., Nielsen, S.B., Mair, K., Di Toro, G., 2013. Mirror-like
1099 faults and power dissipation during earthquakes. Geology. http://dx.
1100 doi.org/10.1130/G34641.1.
1101
1102 Giorgetti, C., Carpenter, B.M., Collettini, C., 2015. Frictional behavior of talc-calcite mixtures, J.
1103 Geophys. Res. Solid Earth, 120, doi:10.1002/ 2015JB011970.
1104

Gomberg, J., 2018. Unsettled earthquake nucleation. Nat. Geosci. 11, 461-466, https://doi.org/10.1038/s41561-018-0149-x.

Gratier, J.P., Gamond, J.F., 1990. Transition between seismic and aseismic deformation in the upper crust. Geological Society of London, Special Publication 54, 461-473.

Gratier, J.P., Richard, J., Renard, F., Mittempergher, S., Doan, M.L., Di Toro, G., Hadizadeh, J., Boullier, A.M., 2011. Aseismic sliding of active faults by pressure solution creep: Evidence from the San Andreas Fault observatory at depth. Geology 39, 1131–1134.

Gratier, J.-P., Dysthe, D.K., Renard, F., 2013. Chapter 2: The role of pressure solution creep in the ductility of the Earth's upper crust. Advances in Geophysics, edited by R. Dmowska, 47–179, Elsevier.

Haines, S., Marone, C., Saffer, D., 2014. Frictional properties of low-angle normal fault gouges and implications for low-angle normal fault slip. Earth and Planetary Science Letters 408, 57–65.

Handy, M.R., 1990. Thesolid-staftleowofpolymineralic rocks. J. Geophys Res. 95, 8647-86611.

Hardebeck, J.L., Loveless, J.P., 2018. Creeping subduction zones are weaker than locked subduction zones. Nat. Geosci. https://doi.org/10.1038/s41561-017-0032-1.

Hayman, N.W., 2006. Shallow crustal rocks from the Black Mountains detachments, Death Valley, CA. Journal of Structural Geology 28, 1767–1784.

Heesakkers, V., Murphy, S., Reches, Z., 2011. Earthquake rupture at focal depth, Part I: Structure and rupture of the Pretorius fault, TauTona mine, South Africa. Pure and Applied Geophysics, 168, 2395-2425.

Holdsworth, R.E. 2004. Weak faults—rotten cores. Science, 303, 181–182.

Holdsworth, R.E., van Diggelen, E.W.E., Spiers, C.J., de Bresser, J.H.P., Walker, R.J., Bowen, L., 2011. Fault rocks from the SAFOD core samples: Implications for weakening at shallow depths along the San Andreas Fault, California. Journal of Structural Geology 33, 132-144, doi:10.1016/j.jsg.2010.11.010.

Hubbert, M., Rubey, W., 1959. Role of fluid pressure in mechanics of overthrust faulting. Geol. Soc. Am. Bull. 70, 115–166.

Ide, S., Baltay, A., Beroza, G.C., 2011. Shallow dynamic overshoot and energetic deep rupture in the 2011 Mw 9.0 Tohoku-Oki earthquake. Science 332, 1426–1429.

Ikari, M., Saffer, D. M., Marone, C., 2009. Frictional and hydrologic properties of clay-rich fault gouge. Journal of Geophysical Research 114, B05409. https://doi.org/10.1029/2008JB006089.

Ikari, M.J., Marone, C., Saffer, D.M., 2011. On the relation between fault strength and frictional stability. Geology 39, 83–86, doi: 10.1130/G31416.1.

Ikari, M.J., Kameda, J., Saffer, D.M., Kopf, A.J., 2015. Strength characteristics of Japan Trench borehole samples in the high-slip region of the 2011 Tohoku-Oki earthquake. Earth and Planetary Science Letters 412, 35–41, http://dx.doi.org/10.1016/j.epsl.2014.12.014.

Imber, J., Holdsworth, R.E., Butler, C.A., Lloyd, G.E., 1997. Fault-zone weakening processes along the reactivated outer hebrides fault zone, Scotland. Journal of the Geological Society of London 154, 105-109.

Jackson, J.A., White, N.J., 1989. Normal faulting in the upper continental crust: Observations from regions of active extension. Journal of Structural Geology 11, 15–36.

Janecke, S.U., Evans, J.P., 1988. Feldspar-influenced rock rheologies. Geology 16, 1064–1067.

Jefferies, S.P., Holdsworth, R.E., Wibberley, C.A.J., Shimamoto, T., Spiers, C.J., Niemeijer, A.R., Lloyd, G.E., 2006. The nature and importance of phyllonite development in crustal-scale fault cores: an example from the Median Tectonic Line, Japan. Journal of Structural Geology 28, 220-235.

Kaduri, M., Gratier, J.P., Renard, F., Çakir, Z., Lasserre, C., 2017. The implications of fault zone transformation on aseismic creep: Example of the North Anatolian Fault, Turkey. J. Geophys. Res. Solid Earth 122, doi:10.1002/2016JB013803.

Kameda, J., Shimizu, M., Ujiie, K., Hirose, T., Ikari, M., Mori, J., Oohashi, K., Kimura, G., 2015. Pelagic smectite as an important factor in tsunamigenic slip along the Japan Trench. Geology, 43, 155-158.

Kaneko, Y., Avouac, J.P., Lapusta N., 2010. Towards inferring earthquake patterns from geodetic observations of interseismic coupling. Nat. Geosci. 3, 363–369.

Cappa, F., Scuderi M.M., Collettini, C., Guglielmi, Y., Avouac, J.P., 2019. Stabilization of fault slip by fluid injection in the laboratory and in situ. Science Advances, doi: 10.1126/sciadv.aau4065.

Kato, A., Obara, K., Igarashi, T., Tsuruoka, H., Nakagawa, S., Hirata, N., 2012. Propagation of slow slip leading up to the 2011 Mw 9.0 Tohoku-Oki earthquake. Science 335(6069), 705–708, doi:10.1126/science.1215141.

Kimura, G., Yamaguchi, A., Hojo, M., Kitamura, Y., Kameda, J., Ujiie, K., Hamada, Y., Hamahashi, M., Hina, S., 2012. Tectonic mélange as fault rock of subduc- tion plate boundary. Tectonophysics 568–569, 25–38. http://dx.doi.org/10.1016/ j.tecto.2011.08.025.

Kirkpatrick, J.D., Rowe, C.D., White, J.C., Brodsky, E.E., 2013. Silica gel formation during fault slip: evidence from the rock record. Geology 41 (9), 1015-1018.

Koopman, A., 1983. Detachment tectonics in the Central Apennines, Italy. Geologica Ultraiectina 30, 1-155.

Lacroix, B., Buatier, M., Labaume, P., Travè, A., Dubois, M., Charpentier, D., Ven- talon, S., Convert-Gaubier, D., 2011. Tectonic and geochemical characterization of thrusting in a

foreland basin: example of the South-Pyrenean orogenic wedge (Spain). J. Struct. Geol. 33, 1359–1377. http://dx.doi.org/10.1016/j.jsg. 2011.06.006.

Lacroix, B., Tesei, T., Oliot, E., Lahfid, A., Collettini, C., 2015. Early weakening processes inside thrust fault.Tectonics, 34, 1396–1411, doi:10.1002/ 2014TC003716.

Lay, T., Kanamori, H., Ammon, C.J., Koper, K.F., Hutko, A.R., Ye, L., Yue, H., Rushing, T.M., 2012. Depth-varying rupture properties of subduction zone megathrust faults. J. Geophys. Res., 117, B04311, doi:10.1029/2011JB009133.

Lockner, D.A., Morrow, C., Moore, D., Hickman, S., 2011. Low strength of deep San Andreas fault gouge from SAFOD core. Nature 472, 82–86, doi:10.1038/nature09927.

Logan, J.M., Friedman, M., Higgs, M., Dengo, C., Shimamoto, T., 1979. Experimental studies of simulated gouge and their application to studies of natural fault zones, in Proceedings of the VIII Conference, Analysis of Actual Fault Zones, Bedrock, U.S. Geol. Survey, Menlo Park, CA, pp. 305–343.

Logan, J.M., Rauenzahn, K.A., 1987. Frictional dependence of gouge mixtures of quartz and montmorillonite on velocity, composition and fabric. Tectonophysics, 144, 87-108.

Manatschal, G., 1999. Fluid-and reaction-assisted low-angle normal faulting: evidence from rift-related brittle fault rocks in the Alps (Err nappe, eastern Switzerland). Journal of Structural Geology 21, 777–793.

Marone, C., 1998a. Laboratory-derived friction laws and their application to seismic faulting. Annu. Rev. Earth Planet. Sci. 26, 643–696. http://dx.doi.org/10.1146/ annurev.earth.26.1.643.

Marone, C., 1998b. The effect of loading rate on static friction and the rate of fault healing during the earthquake cycle. Nature, 391, 69–72, doi:10.1038/34157.

McClay, K. R., Coward, M.P., 1981. The Moine Thrust Zone: an overview. Geological Society, London, Special Publications, 9, 241-260. https://doi.org/10.1144/GSL.SP.1981.009.01.22

Meneghini, F., Moore, J.C., 2008. Deformation and hydrofracture in a subduction thrust at seismogenic depths: The Rodeo Cove thrust zone, Marin Headlands, California. GSA Bulletin; 119, 174–183, doi: 10.1130/B25807.1.

Miller, S.A., Nur, A., Olgaard, D.L., 1996. Earthquakes as coupled shear stress–high pore pressure dynamical system. Geophys. Res. Lett. 23, 197–200.

Moore, D.E., Lockner, D.A., 2004. Crystallographic control of the frictional behavior of dry and water-saturated sheet structure minerals, J. Geophys. Res. 109, doi:10.1029/2003JB002582.

Moore, D.E., Lockner, D.A., 2007. Friction of the smectite clay mont- morillonite, in The Seismogenic Zone of Subduction Thrust Faults, edited by T. Dixon and C. Moore 317–345, Columbia Univ. Press, New York.

Moore, D.E., Lockner, D.A., Hickman, S. 2016. Hydrothermal frictional strengths of rock and mineral samples relevant to the creeping section of the San Andreas Fault. Journal of

Structural Geology 89, 153-167, http://dx.doi.org/10.1016/j.jsg.2016.06.005.

Morley, C.K., von Hagke, C., Hansberry, R.L., Collins, A.S., Kanitpanyacharoen, W., King, R. 2017. Review of major shale-dominated detachment and thrust characteristics in the diagenetic zone: Part I, meso-and macro-scopic scale. Earth-Science Reviews 173, 168-228, https://doi.org/10.1016/j.earscirev.2017.07.019.

Niemeijer, A.R., Spiers, C.J., 2005. Influence of phyllosilicates on fault strength in the brittle–ductile transition: insights from rock analogue experiments. In Bruhn, D. & Burlini, L. (eds). High-Strain Zones: Structure and Physical Properties. Geological Society, London, Special Publications, 245, 303–327.

Niemeijer, A.R., Spiers, C.J., 2007. A microphysical model for strong velocity weakening in phyllosilicate-bearing fault gouges. J. Geophys. Res. 112, B10405. http://dx.doi.org/10.1029/2007JB005008.

Niemeijer, A. R., Marone, C., D. Elsworth, D., 2010. Fabric induced weakness of tectonic faults. GRL, 37, L03304, doi:10.1029/2009GL041689.

Noda, H., Lapusta, N., 2013. Stable creeping fault segments can become destructive as a result of dynamic weakening. Nature 493, 518–521.

Platt, J.P., Vissers, R.L.M., 1980. Extensional structures in anisotropic rocks. Journal of Structural Geology, 2, 397-410, https://doi.org/10.1016/0191-8141(80)90002-4.

Plümper, O., Røyne, A., Magrasó, A., Jamtveit, B., 2012. The interface-scale mechanism of reaction-induced fracturing during serpentinization. Geology 2012, 40, 1103–1106.

Price, R.A., 1988. The mechanical paradox of large overthrusts. Geological Society of America Bulletin 100 (12), 1898-1908.

Ramsay, J.G., Graham, R.H., 1970. Strain variations in shear belts. Canadian Journal of Earth Sciences 7, 786-813, http://dx.doi.org/10.1139/e70-078.

Renard, F., Voisin, C., Marsan, D., Schmittbuhl, J., 2006. High resolution 3D laser scanner measurements of a strike–slip fault quantify its morphological anisotropy at all scales. Geophys. Res. Lett. 33, L04305. doi:10.1029/2005GL025038.

Rice, J.R., 1992. Fault stress state, pore pressure distribution, and the weakness of the San Andreas Fault, in Fault mechanics and transport properties of the rocks. In: Evans, B., Wong, T.F. (Eds.), A Festschrift in Honour of W.F. Brace. Academic, San Diego, CA, 475–503.

Rice, J.R., 2006. Heating and weakening of faults during earthquake slip. Journal of Geophysical Research, Solid Earth 111 (B5).

Rice, JR., Dunham, E.M., Noda, H., 2009. Thermo- and hydro-mechanical processes along faults during rapid slip. In Meso-scale shear physics in earthquake and landslide mechanics, ed. Y. Hatzor, J. Sulem, and I. Vardoulakis, 3-16. Boca Raton: CRC Press.

Rowe, C.D., Meneghini, F., Moore, J.C., 2011. Textural record of the seismic cycle: strain rate variation in an ancient subduction thrust. In: Geology of the Earthquake Source: a Volume in Honour of Richard Sibson. Vol. 359. Journal of the Geological Society Special Publication, pp. 77-95.

Rowe, C. D., Fagereng, Å. ., Miller, J.A., Mapani, B., 2012. Signature of coseismic decarbonation in dolomitic fault rocks of the Naukluft Thrust, Namibia. Earth Planet. Sci. Lett. 333, 200–210.

Rowe, C.D., Moore, C.J., Remitti, F., the IODP Expedition 343/343T Scientists, 2013. The thickness of subduction plate boundary faults from the seafloor into the seismogenic zone. Geology 41, 991-994.

Rowe, C.D., Griffith, W.A., 2014. Do faults preserve a record of seismic slip: A second opinion. Journal of Structural Geology 78, 1-26.

Rubin, A.M., Gillard, D., Got, J.L., 1999. Streaks of microearthquakes along creeping faults. Nature 400, 635–641.

Ruina, A., 1983. Slip instability and state variable friction laws. J. Geophys. Res. 88, 10359–10370, http://dx.doi.org/10.1029/JB088iB12p10359.

Ruiz, S., Metois, M., Fuenzalida, A., Ruiz, J., Leyton, F., Grandin, R., Vigny, C., Madariaga, R., Campos, J., 2014. Intense foreshocks and a slow slip event preceded the 2014 Iquique Mw 8.1 earthquake. Science 345(6201), 1165–1169, doi:10.1126/science.1256074.

Rutter, E.H., Faulkner, D.R., Burgess, R., 2012. Structure and geological history of the Carboneras Fault Zone, SE Spain: Part of a stretching transform fault system. Journal of Structural Geology 45, 68-86.

Saffer, D. M., Marone, C., 2003. Comparison of smectite- and illite-rich gouge frictional properties: Application to the updip limit of the seismogenic zone along subduction megathrusts. Earth Planet. Sci. Lett., 215, 219–235, doi:10.1016/S0012-821X(03)00424-2.

Sagy, A., Brodsky, E.E., Axen, G.J., 2007. Evolution of fault-surface roughness with slip. Geology 35, 283–286.

Schleicher, A. M., van der Pluijm, B., Warr, L. N., 2010. Nanocoatings of clay and creep of the San Andreas fault at Parkfield, California. Geology 38, 667–670.

Schoenball, M., Ellsworth, W.L., 2017. A systematic assessment of the spatio- temporal evolution of fault activation through induced seismicity in Oklahoma and southern Kansas. Journal of Geophysical Research: Solid Earth 122, 10,189–10,206, doi.org/10.1002/2017JB014850.

Scholz, C.H., Small, C., 1997. The effect of seamount subduction on seismic coupling. Geology 25, 487–490.

Scholz, C. H., 2002. The Mechanics of Earthquakes and Faulting, 2nd ed., Cambridge Press, New York.

1353 Scuderi, M.M., Collettini, C., Viti, C., Tinti, E., Marone, C., 2017. Evolution of shear fabric in
1354 granular fault gouge from stable sliding to stick slip and implications for fault slip mode.
1355 Geology doi:10.1130/G39033.1.
1356
1357 Shea, W.T.J., Kronenberg, A.K., 1993. Strength and anisotropy of foliated rocks with varied
1358 mica contents. J. Struct. Geol. 15, 1097–1121.
1359
1360 Shipton, Z.K., Cowie, P.A., 2001. Damage zone and slip-surface evolution over mm to km scales
1361 in high-porosity Navajo sandstone, Utah. Journal of Structural Geology 23 (12), 1825-1844.
1362
1363 Sibson, R.H., 1974. Frictional constraints on thrust, wrench and normal faults. Nature 264,
1364 542-544.
1365
1366 Sibson, R., 1977. Faults rocks and fault mechanisms. J. Geol. Soc. (Lond.) 133, 191–213.
1367 https://doi.org/10.1144/gsjgs.133.3.0191.
1368
1369 Sibson, R.H., 1985. A note on fault reactivation. J. Struct. Geol. 7, 751–754.
1370
1371 Sibson, R.H., 1992. Implications of fault-valve behaviour for rupture nucleation and
1372 recurrence. Tectonophysics, 211, 283-293, https://doi.org/10.1016/0040-1951(92)90065-E.
1373
1374 Sibson, R.H., and Xie, G., 1998, Dip range for intracontinental reverse fault ruptures: Truth not
1375 stranger than friction?. Seismological Society of America Bulletin 88, 1014–1022.
1376
1377 Sibson, R.H., 2003. Thickness of the Seismic Slip Zone. Bulletin of the Seismological Society of
1378 America 93(3), 1169–1178.
1379
1380 Sibson, R.H., 2009. Rupturing in overpressured crust during compressional inversion—the
1381 case from NE Honshu, Japan. Tectonophysics 473, 404–416.
1382
1383 Sibson, R.H., 2017. Tensile overpressure compartments on low-angle thrust faults. Earth,
1384 Planets and Space DOI 10.1186/s40623-017-0699-y.
1385
1386 Siman-Tov, S., Aharonov, E., Sagy, A., Emmanuel, S., 2013. Nanograins form carbonate fault
1387 mirrors. Geology 41, 703–706.
1388
1389 Smith, S.A.F., Bistacchi, A., Mitchell, T.M., Mittemperger, S., Di Toro, G., 2013. The structure of
1390 an exhumed intraplate seismogenic fault in crystalline basement. Tectonophysics 599, 29–44,
1391 http://dx.doi.org/10.1016/j.tecto.2013.03.031.
1392
1393 Smith, S.A.F., Tesei, T., Scott, J.M., Collettini, C., 2017. Reactivation of normal faults as high-
1394 angle reverse faults due to low frictional strength: Experimental data from the Moonlight
1395 Fault Zone, New Zealand. Journal of Structural Geology 105, 34–43.
1396
1397 Solum, G.S., van der Pluijm, B.A., 2009. Quantification of fabrics in clay gouge from the
1398 Carboneras fault, Spain and implications for fault behavior. Tectonophysics 475, 554–562,
1399 doi:10.1016/j.tecto.2009.07.006.
1400
1401 Spray, J.G., 2010. Frictional melting processes in planetary materials: from hyper- velocity
1402 impacts to earthquakes. Annu. Rev. Earth Planet. Sci. 38, 221-254,

http://dx.doi.org/10.1146/annurev.earth.031208.100045.

Suppe, J., 2007. Absolute fault and crustal strength from wedge tapers. Geology 35, 1127–1130, doi:10.1130/G24053A.1.

Swanson, M.T., 2006. Pseudotachylyte-bearing strike-slip faults in mylonitic host rocks, Fort Foster Brittle Zone, Kittery, Maine. Earthquakes: Radiated Energy and the Physics of Faulting 170, 167–179.

Takahashi, M., Mizoguchi, K., Kitamura, K., Masuda, K., 2007. Effects of clay content on the frictional strength and fluid transport property of faults, J. Geophys. Res., 112, B08206, doi:10.1029/2006JB004678.

Tape, C., Holtkamp, S., Silwal, S., Hawthorne, J., Kaneko, Y., Ampuero, J.P., Ji, C., Ruppert, N., Smith, K., West, M.E., 2018. Earthquake nucleation and fault slip complexity in the lower crust of central Alaska. Nat. Geosci. https://doi.org/10.1038/s41561-018- 0144-2.

Tarling, M.S., Smith, S.A.F., Viti, C., Scott, J.M., 2018. Dynamic earthquake rupture preserved in a creeping serpentinite shear zone. Nature Communications, DOI: 10.1038/s41467-018-05965-0.

Tchalenko, J.S., 1970. Similarities between Shear Zones of Different Magnitudes. Geological Society of America Bulletin 81, 1625-1640.

Tembe, S., Lockner, D.A., Wong, T.F., 2010. Effect of clay content and mineralogy on frictional sliding behavior of simulated gouges: Binary and ternary mixtures of quartz, illite, and montmorillonite. J. Geophys. Res., 115, B03416, doi:10.1029/2009JB006383.

Tenthorey, E., Cox, S.F., Todd, H.F., 2003. Evolution of strength recovery and permeability during fluid-rock reaction in experimental fault zones. Earth Planet. Sci. Lett., 206(1–2), 161–172, doi:10.1016/S0012-821X(02)01082-8.

Tesei, T., Collettini, C., Carpenter, B.M., Viti, C., Marone, C., 2012. Frictional strength and healing behavior of phyllosilicate-rich faults. J. Geophys. Res. Solid Earth 117, B09402, doi:10.1029/2012JB009204.

Tesei, T., Collettini, C., Viti, C., Barchi, M.R., 2013. Fault architecture and deformation mechanisms in exhumed analogues of seismogenic carbonate-bearing thrusts. J. Struct. Geol. 55. http://dx.doi.org/10.1016/j.jsg.2013.07.007.

Tesei, T., Collettini, C., Barchi, M.R., Carpenter, B.M., Di Stefano, G., 2014. Heterogeneous strength and fault zone complexity of carbonate-bearing thrusts with possible implications for seismicity: Earth and Planetary Science Letters, 408, 307–318, doi:10.1016/j.epsl.2014.10.021.

Tesei, T., Lacroix, B., Collettini, C., 2015. Fault strength in thin-skinned tectonic wedges across the smectite-illite transition: constraints from friction experiments and critical tapers. Geology, doi:10.1130/G36978.1

1453 Tesei, T., Harbord, C. W. A., De Paola, N., Collettini, C., Viti, C., 2018. Friction of mineralogically
1454 controlled serpentinites and implications for fault weakness. Journal of Geophysical Research:
1455 Solid Earth, 123. https://doi.org/10.1029/ 2018JB016058.
1456
1457 Townend, J., Zoback, M.D., 2000. How faulting keeps the crust strong. Geology 28(5),399–402.
1458
1459 Vannucchi, P., F. Sage, Phipps Morgan, J., Remitti,G., Collot, Y.J., 2012. Toward a dynamic
1460 concept of the subduction channel at erosive convergent margins with implications for
1461 interplate material transfer. Geochem. Geophys. Geosyst., 13, Q02003,
1462 doi:10.1029/2011GC003846.
1463
1464 Verberne, B.A., He, C., Spiers, C.J., 2010. Frictional properties of sedi- mentary rocks and
1465 natural fault gouge from the Longmenshan Fault Zone, Sichuan, China,.Bull. seism. Soc. Am.
1466 100, 2767–2790.
1467
1468 Viti, C., Collettini, C., 2009. Growth and deformation mechanisms of talc along a natural fault: a
1469 micro/nanostructural investigation. Contrib Mineral Petrol 158, 529–542.
1470
1471 Viti, C., Collettini, C., Tesei, T., 2014. Pressure solution seams in carbonatic fault rocks:
1472 mineralogy, micro/nanostructure and deformation mechanism. Contrib. Mineral. Petrol. 167.
1473 http://dx.doi.org/10.1007/s00410-014-0970-1.
1474
1475 Viti, C., Collettini, C., Tesei, T., Tarling, M., Smith, S.A.F., 2018. Deformation processes, textural
1476 evolution and weakening in retrograde serpentinites. Minerals 8, 241,
1477 doi:10.3390/min8060241.
1478
1479 Warr, L.N., Wojatschke, J., Carpenter, B.M., Marone, C., Schleicher, A.N., van der Pluijm, B.A.,
1480 2014. A “slice-and-view” (FIBeSEM) study of clay gouge from the SAFOD creeping section of
1481 the San Andreas Fault at ~2.7 km depth. Journal of Structural Geology 69, 234-244.
1482
1483 Waldhauser, F., Ellsworth, W.L., Schaff, D.P., Cole, A., 2004. Streaks, multiplets, and holes:
1484 High-resolution spatiotemporal behavior of Park- field seismicity. Geophys. Res. Lett., 31,
1485 L18608, doi:10.1029/ 2004GL020649.
1486
1487 Wallis, D., Lloyd, G.E., Phillips, R.J., Parsons, A.J., Walshaw, R.D., 2015. Low effective fault
1488 strength due to frictional-viscous flow in phyllonites, Karakoram Fault Zone, NW India.
1489 Journal of Structural Geology, 77, 45-61.
1490
1491 Walsh, F.R., Zoback, M.D. (2016). Probabilistic assessment of potential fault slip related to
1492 injection-induced earthquakes: Application to north-central Oklahoma, USA. Geology 44(12),
1493 991–994, doi.org/10.1130/G38275.1.
1494
1495 Wang, K., Bilek, S.L., 2014. Invited review paper: Fault creep caused by subduction of rough
1496 seafloor relief. Tectonophysics 610, 1–24.
1497
1498 Weeks, J.D. , Tullis, T.E., 1985. Frictional sliding of dolomite: a variation in constitutive
1499 behaviour. J. Geophys. Res. 90, 7821–7826.
1500
1501 Wernicke, B., 1981. Low angle normal faults in the Basin and Range Province: Nappe tectonics
1502 in an extending orogene. Nature 291, 645–648.

Wibberley, C.A.J., 1999. Are feldspar-to-mica reactions necessarily reaction- softening processes in fault zones? Journal of Structural Geology 21, 1219–1227.

Wibberley, C.A.J., Shimamoto, T., 2003. Internal structure and permeability of major-slip fault zones: the Median Tectonic Line in Mie Prefecture, Southwest Japan. Journal of Structural Geology 25, 59–78.

Wibberley, C.A.J., 2005. Initiation of basement thrust detachments by fault-zone reaction weakening. Geological Society, London, Special Publications, 245, 347-372.

Wibberley, C.A.J., Yielding, G., Di Toro, G., 2008. Recent advances in the under- standing of fault zone internal structure; a review. In: Wibberley, C.A.J., Kurz, W., Imber, J., Holdsworth, R.E., Collettini, C. (Eds.), Structure of Fault Zones: Implications for Mechanical and Fluid-flow Properties. Geological Society of London Special Publication 299, 5-33.

Wintsch, R.P., Christoffersen, R., Kronenberg, A.K., 1995. Fluid-rock reaction weakening of fault zones. Journal of Geophysical Research 100, 13021-13032.

Wintsch, R.P., Yeh, M.W., 2013. Oscillating brittle and viscous behavior through the earthquake cycle in the Red River Shear Zone: Monitoring flips between reaction and textural softening and hardening. Tectonophysics 587, 46–62.

Worden, R.H., Morad, S., 2000. Quartz Cementation in Oil Field Sandstones: A Review of the Key Controversies. Wiley Online Library https://doi.org/10.1002/9781444304237.ch1

Zoback, M.D., et al., 1987. New evidence on the state of stress of the San Andreas fault system. Science 238, 1105–1111.

Zoback, M.D., Healy, J.H., 1984. Friction, faulting, and “in situ” stresses. Annales Geophysicae 2, 689–698.

Zoback, M.D., 2010. Reservoir Geomechanics. Cambridge University Press, 449 p.

Zoback, M.D., Hickman, S.H., Ellsworth, B., 2010. Scientific drilling into the San Andreas fault zone. Eos: Transactions of the American Geophysical Union 91 (22), 197-199.

1541

1542 Table 1. Examples of fault zone structures characterized by interconnected networks of
1543 phyllosilicates formed during the fault activity.

Fault	Depth	Protolith	Phyllosilicates	References
Carboneras, Spain	2-4 km	Mica schists	Chlorite, illite	Faulkner et al., 2003; Solum and van der Pluijm, 2009
San Andreas at SAFOD, US	3 km	Serpentinites	Smectite clays (saponite)	Schleicher et al., 2010; Holdsworth et al., 2011
Midian Tectonic Line, Japan	5-10 km	Granitoids	Chlorite, muscovite	Jefferies et al., 2006
North Anatolian Fault, Turkey	< 5 km	Dolomite, quartz & calcite rich rocks	Talc, kaolinite & chlorite.	Kaduri et al., 2017
Livingstone fault, New Zealand	300–350 °C	Ultramafic rocks	Lizardite, chrysotile	Tarling et al., 2018
Rodeo Cove, California	8-10 km	Basalts	Chlorite	Meneghini & Moore, 2008
Thrusts in the Apennines	1-4 km	Marly limestone	Illite, smectite	Tesei et al., 2013
Perdido thrust Pyrenees	6-7 km	Limestones and sandstone	Illite, chlorite	Lacroix et al., 2011
Chrystalls Beach mélange New Zealand	T < 300°C	Sandstone and metabasalts	Illite, muscovite	Fagereng and Cooper, 2010; Fagereng and Sibson, 2010
M. Fico thrust Italy	T < 300°	Ultramafic rocks	Lizardite, chrysotile & polygonal serpentine	Viti et al., 2018; Tesei et al., 2018
Wasatch and Dixie valley faults, US	< 10 km	Quartz-feldspatic rocks	Muscovite, chlorite & clays	Bruhn et al., 1994
Zuccale fault Italy	4-6 km	Dolostone	Talc & smectite	Viti and Collettini., 2009
Black Mountains Detachment, California	From > 3 km to shallow	Carbonate, siliceous gneisses quartz-feldspatic basement, volcanic rocks	Illite, chlorite, smectite & saponite	Hayman, 2006
Gubbio Fault, Apennines	< 4 km	Limestone and	Illite & smectite	Bullock et al., 2014

		marly limestones		
Err Nappe, Switzerland	< 300°C	Quartz-feldspatic rocks	60% chlorite illite in the fault core	Manatschal, 1999

1544

1545

1546 Table 2. Frictional properties of phyllosilicate-rich faults; w = wafer experiments, p powder
1547 experiments.
1548

Fault & weak minerals	Normal stress, Temperature	Friction	(a-b) 0.01-300 μm/s	Healing rate β	Reference
Moonlight (NZ), chlorite	5-75 MPa T = 25° C, wet	0.24 w			Smith et al., 2017
Moonlight (NZ), muscovite	5-50 MPa T = 25° C, wet	0.19 w			Smith et al., 2017
M. Fico Thrust (ITA) chrysotile & Pol. serpentine	20-100 MPa T = 170° C, wet	0.19 p			Tesei et al., 2018
M. Fico Thrust (ITA) chrysotile & Pol. serpentine	5-100 MPa T = 25° C, wet	0.15 p			Tesei et al., 2018
M. Fico Thrust (ITA) lizardite	20-100 MPa T = 170° C, wet	0.18 p			Tesei et al., 2018
M. Fico Thrust (ITA) lizardite	5-100 MPa T = 25° C, wet	0.18 p			Tesei et al., 2018
Perdido thrust (SPA) illite, chlorite	10-75 MPa T = 25° C, wet	0.17 w	0.0050-0.0052	$\beta \approx 0.0008$	Tesei et al., 2015
Coscerno thrust (ITA) smectite	10-100 MPa T = 25° C, wet	0.27 w	0.0038-0.0095	$-0.001 < \beta < 0.003$	Tesei et al., 2014
Zuccale normal fault (ITA), talc & smectite	10-150 MPa T = 25° C, room humidity	0.25-0.31 w	0.0021-0.0087	$0.0002 < \beta < 0.002$	Collettini et al., 2009b; Collettini et al., 2011; Healing Tesei et al., 2012
J-FAST (JPN), smectite	5-7 MPa T = 25° C, wet	0.2-0.26 p	0-0.003		Ikari et al., 2015
SAFOD CDZ (USA) saponite	40-200 MPa, 25-250°C, fluid pressure	0.1-0.17 p	0.0007- 0.0067		Lockner, 2011 Moore et al., 2016
SAFOD SDZ (USA) saponite	40-200 MPa, 25-250°C, fluid pressure	0.15-1-19 p	0.0011-0.007 v. weakening (a few) at T>200°C		Lockner, 2011 Moore et al., 2016
SAFOD CDZ (USA) smectite	25-50 MPa, 25°C, fluid pressure	0.1-0.25 p	0.002–0.008	$-0.0012<\beta<-0.001$	Carpenter et al., 2011 Carpenter et al., 2015
SAFOD SDZ (USA) smectite	25-50 MPa, 25°C, fluid pressure	0.12-0.15 w	-0.0015–0.011	$-0.0023<\beta<0.001$	Carpenter et al., 2011 Carpenter et al., 2015
Alpine Fault (NZ) Gaunt Creek, Illite, chlorite	6 MPa, 25°C, fluid pressure	0.28 p	0.0076–0.0153	$-0.0013<\beta<-0.0004$	Barth et al., 2013
South Alpine Fault (NZ) Martyr River, illite, chlorite.	31 MPa, 25°C, fluid pressure	0.32 p	0.0035–0.0089	$-0.0013<\beta<0.0008$	Barth et al., 2013
South Alpine Fault (NZ) McKenzie Creek, smectite, chlorite, liz.,	6 MPa, 25°C, fluid pressure	0.13 p	0.0051–0.0098	$-0.0017<\beta<0.0001$	Barth et al., 2013
South Alpine Fault (NZ) Hokuri Creek,	6 MPa, 25°C, fluid pressure	0.12 p	0.0049–0.0085	$-0.0003<\beta<-0.00004$	Barth et al., 2013

smectite, chlorite.					
South Alpine Fault (NZ) Hokuri Creek Smectite, lizardite.	31-94 MPa, 25-210 C°, fluid pressure	0.12-0.16 p	0.001-0.007		Boulton et al., 2018
Whipple Mts. Detachment (USA), clay	20-60 MPa, 25 °C, room humidity	0.29-0.30 p			Haines et al., 2014
Panamint Detachment (USA), clay	20-60 MPa, 25 °C, room humidity	0.28-0.38 p			Haines et al., 2014
Waterman Hills detachment (USA), clay	20-60 MPa, 25 °C, room humidity	0.38-0.43 p			Haines et al., 2014

1549